UNIVERSITY OF CALIFORNIA,
IRVINE

Experimental Investigation of Hydrogen and Hydrogen/ Methane Mixture Leakage from Low-Pressure Natural Gas Infrastructure

THESIS

submitted in partial satisfaction of the requirements
for the degree of

MASTER OF SCIENCE

in Mechanical and Aerospace Engineering

by

Nohora Alejandra Hormaza Mejia

Thesis Committee:
Professor Jacob Brouwer, Chair
Associate Professor Vince McDonell
Assistant Professor Donald Dabdub

2019

DEDICATION

To

my family, friends, and professors

in recognition of their worth

an apology

"And what will they burn instead of coal?"
"Water," replied Harding.
"Water!" cried Pencroft, "water as fuel for steamers and engines! Water to heat water!"
"Yes, but water decomposed into its primitive elements," replied Cyrus Harding, "and decomposed doubtless, by electricity, which will then have become a powerful and manageable force, for all great discoveries, by some inexplicable laws, appear to agree and become complete at the same time.
Yes, my friends, I believe that water will one day be employed as fuel, that hydrogen and oxygen which constitute it, used singly or together, will furnish an inexhaustible source of heat and light, of an intensity of which coal is not capable. Someday the coal rooms of steamers and the tenders of locomotives will, instead of coal, be stored with these two condensed gases, which will burn in the furnaces with enormous calorific power.

Jules Verne
"The Mysterious Island"

TABLE OF CONTENTS

LIST OF FIGURES

LIST OF TABLES

AKNOWLEDGMENTS

I would like to express my deepest gratitude to my advisor, Professor Bouwer, and for all of his guidance, mentorship, and support, which made grad school and this research possible and enjoyable.

I would like to thank my committee members, Professor Dabdub and Professor McDonell, for taking time from their busy schedules this quarter to provide valuable feedback on this study.

Finally, I would also like thank the students and staff at the Advanced Power and Energy Program for being part of a wonderful community. Financial support was provided by the University of California, Irvine, the Advanced Power and Energy Program.

ABSTRACT OF THE THESIS

Experimental Investigation of Hydrogen and Hydrogen/ Methane Mixture Leakage from Low-Pressure Natural Gas Infrastructure

By

Alejandra Hormaza Mejia

Master of Science in Mechanical and Aerospace Engineering

University of California, Irvine, 2019

Professor Jacob Brouwer, Chair

A global interest to increase the use of renewable resources has spurred an interest in hydrogen (H_2) gas as an energy carrier. Natural gas (NG) infrastructure has been proposed as a potential storage, transmission and distribution system for renewably produced gaseous H_2 fuel. Introducing H_2 to the NG system has raised concerns about H_2 leakage from the system. In this thesis, the leakage of H_2, NG and H_2/NG blends is theoretically and experimentally examined. Experimental evidence that suggests 100% H_2 gas leaks at the same rate as H_2/ NG mixtures and 100% NG in typical existing low-pressure NG infrastructure on the customer-side of the meter is provided. Additionally, a review of the classical leak analysis literature resulted in the discovery of similar results, though not mentioned in the literature. The efficacy of a commercial mitigation measure to reduce gaseous fuel leakage from piping system known to leak is assessed. Finally, a two-step leakage mechanism theory that involves molecular dynamics and a tortuous leakage path with significant wall interactions is proposed to explain the results that suggest H_2 leaks at the same rate as NG in typical low-pressure gas infrastructure.

1. Introduction: A New Epoch

For hundreds of years, an amazing natural storage of solar energy in the form of oil, coal, and gas has sustained human lives by providing a dense and seemingly everlasting supply of energy. This has allowed humans to achieve great technological and medical advancements that led to exponential growth in population size and longer lives, encouraging further consumption of these resources.

Fossil fuels provided humans with the power to manipulate the flow of all fresh water by the construction of large dams, aquifers, which permitted large populations of humans to settle in places like Los Angeles, which, without altering, could have never sustained the population sizes of today. Amazing improvements in the efficiency, accessibility, and development of transportation is more evidence of the powerful impact fossil fuels have had on humans, which have changed how and where humans live and where humans are able to travel to on a universal level.

On the other hand, consumption of these fossil fuel resources has come at a cost for all things living on Earth. While it took millions of years for these fuels to form into a massive accumulation of solar energy through mechanisms such as photosynthesis, followed by death, decay and millions of years of heat and pressure to produce fossil fuels, humans are depleting these resources in a few generations [1]. Not only are humans exhausting the supply as the population is increasing, consumption of these resources is altering the atmosphere, biodiversity, and Earth in severe, unprecedented ways. The combustion processes of these fuels have resulted in significant emissions of air pollutants which are damaging air quality and health and greenhouse gases and have contributed to

the observed rise in the global average temperature, leading to rising sea levels, melting of glaciers, and have compromised human health.

Additionally, extraction of these fuels has resulted in catastrophic accidents, such as the 2010 British Petroleum oil spill in the Gulf of Mexico, the 2015 gas leak in Aliso Canyon, and the 2008 coal ash spill in Tennessee [2], [3]. As the natural supply of these fossil fuels becomes more scarce, extracting these fuels will become even more challenging increasing the severity of an accident.

Further, the magnitude and longevity of human-induced changes to Earth has reached a level so significant, that humans are now considered to be a major geological force and some geologists are proposing a new epoch: the Anthropocene [1], [4]–[6]. While the specific date of the onset of the "Anthropocene" is debated by scientists, substantial evidence suggests that these effects have become exacerbated since the Industrial Revolution [1], [4].

To continue to sustain the world's appetite for energy, an increasing population and a growing demand for faster, better, more powerful technology, society must transition to more sustainable resources, and to mitigate and reverse this environmental crisis. Massive, unprecedented changes are occurring on Earth at a rate that is much faster than expected; and these changes are causing serious destruction to Earth's natural life-support system. These urgent issues must be fundamentally addressed with a cultural shift in how society converts, distributes, and consumes energy.

The goal of this study is to research how gaseous hydrogen (H_2) fuel, considered to be the "fuel of the future" by some for its capabilities to be produced renewably and to generate electricity at high efficiencies and with zero emissions of both pollutants and

greenhouse gases, may impact our existing natural gas (NG) infrastructure as we begin a transition to more sustainable energy conversion systems.

2 Background

2.1 Challenges of Introducing Renewables

In response to these pressing environmental and societal challenges of the 21st century, and an expected global energy demand increase of 89% between 2012 and 2041, governments around the world are passing rigorous climate and sustainability legislation [7]. For example, the state of California has set aggressive energy and climate goals such as reducing greenhouse gas emission levels to 1990 levels by 2020, generating 60% of the state's total electrical energy from renewables by 2030; generating 100% of the state's energy from zero emissions sources (mostly renewables) by 2045 [8], [9]. Further, the State also passed AB 617 which prioritizes the need to improve the public health of communities disproportionately burdened and affected by exposure to criteria air pollutants and toxic air contaminants [10]. AB 617 establishes community-level air monitoring, state and local emission reduction plans, requirements to report emissions, and penalties for polluters [10]. To increase the fleet of commercial zero emission vehicles on the road, the state has eased weight restrictions on electrical vehicles, allocated funds to expand charging infrastructure for electric vehicles, and has mandated automakers to sell a minimum number of zero emission vehicles (ZEV) or else automakers will face a fine [11], [12]. Similarly, as part of Germany's Energiewende, an ambitious energy transition to a future that is more "secure, environmentally friendly, and economically successful," Germany has set similar goals to reduce greenhouse-gas emissions and adopt more wind and solar power conversion systems: (1) Source 40-45% of its electricity from renewables by 2025 and 80% by 2050; (2) Reduce greenhouse gas emissions by 40% from 1990 levels by 2020 [13]–[15].

To achieve these air quality and climate goals, installation of intermittent and uncontrollable renewable energy resources, mainly solar and wind, and integration of these systems with existing power grids will be essential. In addition, complete decarbonization of transportation fuels, the NG system, fertilizer, cement, and other chemical and industrial processes is required [16]. The US EIA estimates that renewables are the fastest growing electricity generation resource [7]; additionally, in 2016, 60% of all utility scale generation capacity installations were from solar and wind resources in the United States [17]. As more of these variable and intermittent renewable energy technologies are integrated into the electrical grid, utilities and system operators are facing a challenge of balancing the intermittent power supply curve with the time-dependent demand of the grid.

The challenges that arise from the mismatch between the intermittent renewable power supply and time-dependent demand are illustrated in the “duck curves” that were published by the California Independent System Operator (CAISO) [18]. In Figure 1, a single “duck curve” is shown for the state of California for a single day, March 31, and several years. For a single day, March 31, the duck chart in Figure 1 illustrates various forecasts of the net load profiles for various amounts of renewable energy. In Figure 2, various duck curves are shown for different seasons. Note the large anticipated ramp for the summer.

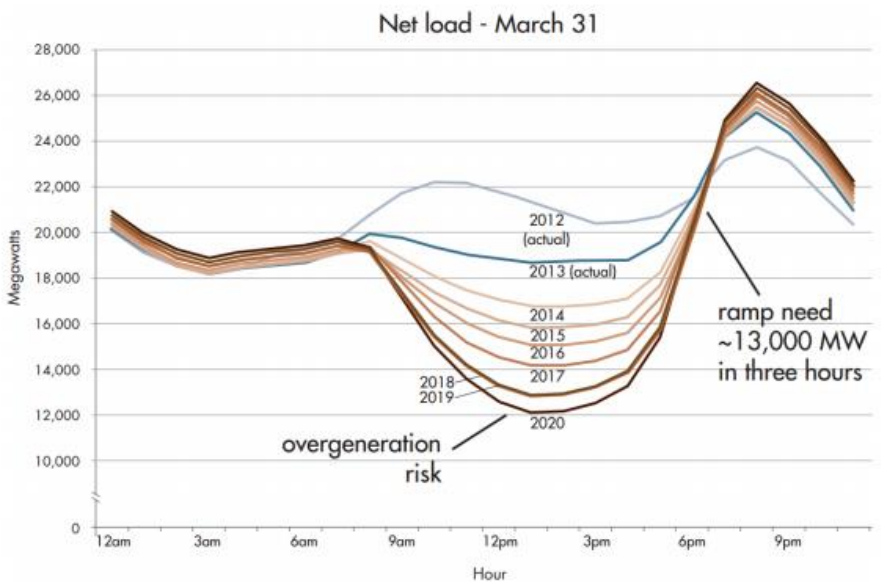

Figure 1: California duck chart (from [18])

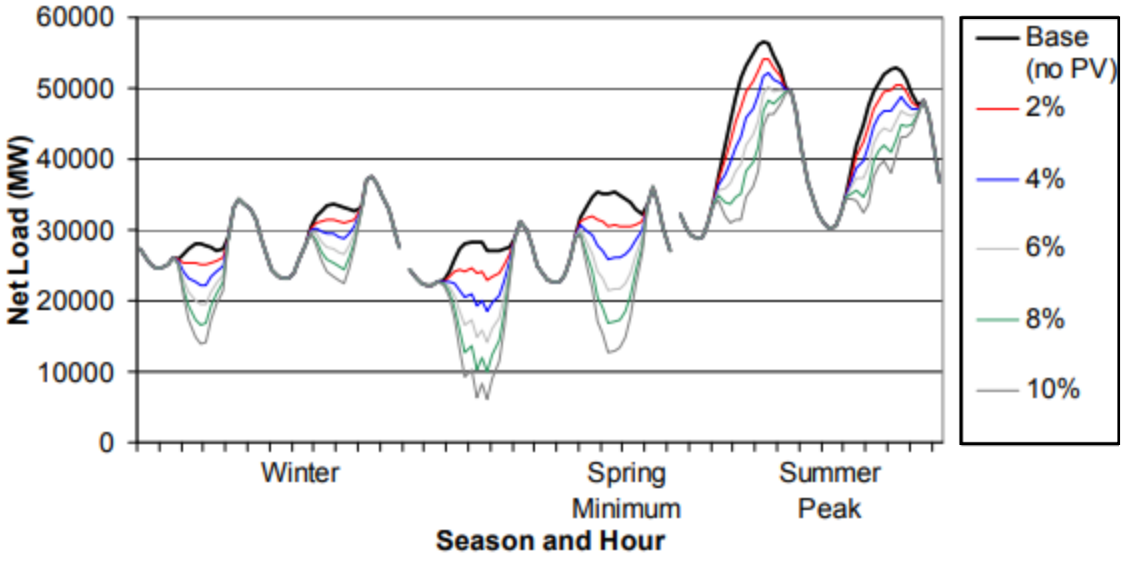

Figure 2: Load shapes in California for various PV penetration scenarios (from [19])

As market penetration of renewable energy increases, the difference between the net load in the middle of the day and in the evening increases substantially, which will require a large upward ramp in the evening to meet the evening peak load. When demand is very

low and the amount of renewable energy available is high, instances of insufficient power system flexibility may occur resulting in curtailed renewable energy or outages [20].

Without proper energy storage, the electrical grid cannot handle the dynamics of intermittent renewable energy resources. Even at moderate levels of renewable energy penetration, the grid must be flexible enough to ramp down in a couple of hours to allow solar energy to be introduced as PV generation increases in the morning [21]. Similarly, in the afternoon when PV generation declines, the grid must be capable of ramping up steeply in a few hours to meet the peak load during the evening. These dynamics may lead to curtailment and overgeneration since the conventional power plants that support the evening load are "long-start resources" that require time to come online and must operate at a minimum power output levels during the middle of the day when nonrenewable electricity is not needed [18]. As more renewables are integrated with the power grid, the magnitude of the upward ramp in the evening hours will increase. If the grid is limited in upward ramping capability, the system operator may have to curtail renewable energy that is produced during the daytime to reduce the magnitude of the upward ramp to avoid load curtailment. Therefore, as market penetration of renewable energy increases, energy storage will play a crucial role in optimizing integration; otherwise, massive curtailment or outages due to insufficient grid flexibility will limit the amount of renewable energy that can be introduced into the grid. Further, these challenges become increasingly difficult with higher levels of renewable energy integration. Eventually very large scale and seasonal energy storage, and zero emissions dispatchable power generation systems will be necessary for successful energy management and for ensuring the highest market penetrations of renewable energy.

An additional challenge that arises from a lack of grid infrastructure flexibility at high levels of renewable energy penetration is negative wholesale electricity pricing. Negative prices due to overgeneration occurred in California on March 16, 2014 in advance of even 33% renewable portfolio standards [21]. The intervals of negative prices occurred between 11am and 5pm when thermal units were ramped down to accommodate solar energy. This problem will only be amplified in the future as more renewables, especially solar, are introduced into the California grid. Therefore, advancing energy storage capabilities to better accommodate and integrate highly available renewables, such as solar and wind into the grid is necessary to meet the rigorous renewable energy goals.

2.1.1 Energy Storage Solutions

Energy storage can help address the enumerated challenges. Some of the energy storage technologies include battery systems, flow (redox) battery systems, flywheels, supercapacitors, superconducting magnetic energy storage, pumped hydro, compressed air, and gaseous fuel energy storage via electrolysis [22]. Though each of these has its unique advantages and drawbacks, the main energy storage systems used for large energy capacity (electric grid scale) systems are pumped hydro, compressed air, and gaseous fuel energy storage. Today, NG is the fuel that is stored in massive underground facilities to support seasonal storage of energy.

2.1.1.1 Battery Systems

The energy storage device most commonly used with PV systems today is the rechargeable lead acid battery [23]. The main advantages of batteries are the high availability of batteries and high consumer confidence in these devices since they have been widely used and accepted by the public. In addition, when batteries are coupled with

PV systems, they can achieve round trip efficiencies up to 90%. The main constraints of batteries include: an energy storage capacity that is limited by battery size; long battery recharging duration; operational limits such as depth of discharge, and low charge rates; relatively short battery life; desolation of the electrodes; and hazardous waste handling during disposal.

2.1.1.2 Flow Batteries

Flow batteries operate on a principle based on a reversible electrochemical reaction that occurs in a set of cells to achieve a desired voltage [22]. Flow batteries store aqueous solutions in external storage tanks. When the battery is in generation mode, the solution will flow through the cells to generate electricity. For flow batteries, energy storage is independent of power capacity, depth of discharge is no longer important, and self-discharge is negligible [24]. Flow batteries are generally best suitable for small and medium scale stationary applications due to their low energy density that requires a large amount of space [22], [24].

2.1.1.3 Flywheels

A flywheel is an electromechanical device that stores kinetic energy according to its change in rotational velocity [22], [24]. Though it has a long life of 15-20 years and is capable of operating with high efficiencies of (90-95%), the self-discharge rate is between 55% and 100%/day, making flywheels most appropriate for uninterruptable power supply or provision of frequency regulation ancillary services rather than long term energy storage [24].

2.1.1.4 Supercapacitors

Supercapacitors electrostatically store energy by accumulating charge on the interface between the surfaces of an electrolyte and the two conductor electrodes [22]. Since capacitors have high power density and low energy density, they are most suitable for fast cycling applications [24]. Supercapacitors have a long life (8 -10 years), high efficiencies (95%), deep discharge/ overcharge capabilities, and high-power densities (10,000 W/kg). Supercapacitors, however, have a high energy dissipation rate (5-40%/day) and high cost, making them most suitable for short time scale applications with short time responses.

2.1.1.5 Superconducting Magnetic Energy Storage System

A superconducting magnetic energy storage system is based on storing energy in a magnetic field, that is generated by flowing direct current through superconducting coil [24]. It is capable of absorbing or injecting large amounts of power in a short time [22]. High costs and advances in other power electronics, have limited the commercialization of these systems [25].

2.1.1.6 Pumped Hydropower

Pumped hydropower energy storage uses height differences in water levels to store potential energy [24]. Pumped hydro can provide high efficiencies, up to 85%, and has a large energy storage capacity, and a long life at a low cycle cost. Some advantages of hydropower are that it has separate power and energy scaling (i.e., pump and turbine sized for power amount, and lakes sized for energy amount) allowing for very large energy storage magnitude for any given power magnitude. Hydro-power responds quickly and can absorb some of the fluctuations of intermittent renewable energy resources, such as

wind power. Hydropower is mainly used for very large (grid scale) energy storage applications since it has a high capital cost and is a limited resource (need available land and steep elevation change) and can have adverse environmental consequences (i.e., building of dams, flooding of the land to make reservoirs).

2.1.1.7 Compressed Air Energy Storage

Compressed air energy storage typically uses an existing underground site, such as a salt dome to store gas at 4 -8 mPA [24]. Similar to pumped hydro, compressed air energy storage also has a high power capacity (up to 300MW), large energy storage capacity (50+h), quick start up, long storage period (over 1 year) , and a relatively high efficiency (up to 80%) [24]. However, to economically justify the coupling of compressed air energy storage with variable renewable energy resources, it must be capable of providing multiple functions, such as peak shaving, regulation control, and smoothing wind variations.

2.1.1.8 Gaseous Fuel Energy Storage and Power-to-Gas

As mentioned previously, NG is pumped into and extracted from various underground storage facilities today to accomplish very large amounts of energy storage (e.g., seasonal storage). Gaseous fuel energy storage via electrolysis is a method of energy storage that has gained momentum internationally and is known also as Power-to-Gas (P2G) or Power-to-Gas-to-Power (P2G2P). P2G has been proposed as a massive and seasonal energy storage solution to support electrical grid management with very high renewable use. The concept of P2G entails storing mostly otherwise curtailed renewable energy as a gaseous fuel through water electrolysis. The gaseous fuel, hydrogen (H_2), is mostly produced using renewable power during peak renewable production times and/or when grid demand is low. One of the main advantages of using gas as an energy storage

medium is that the energy storage capacity is scaled independently from power capacity, since energy scales with H_2 storage size independent of power which scales with electrolyzer and fuel cell size, unlike batteries which come with a fixed power/energy ratio [23]. The construction of power-to-gas sites can be less invasive than pumped hydropower storage sites. P2G can also be more cost-effective than Lithium-ion ion batteries for large energy capacity and more geographically flexible than pumped hydro and compressed air, which are the two main storage technologies currently in use or considered for massive energy capacity systems [26]. Finally, if H_2 is able to replace fossil fuels in difficult to electrify applications (e.g., heavy duty transport, shipping, aviation, chemicals, cement, industry), H_2 has the potential to perpetually contribute to a totally zero emissions economy [16].

Recent efforts to increase renewable energy penetration has spurred an international interest to pursue P2G especially in Europe where over 30 projects are installed or are in development that total 100+ MW in size [26]. Pilot plants are already under construction or in operation in Germany, Switzerland, Denmark, the United Kingdom, Spain, Italy, the Netherlands, Belgium, Austria and France (e.g., see [26]–[32]).

One of the most prominent countries advancing the P2G concept is Germany, partly due to their long-term plan for sustainable energy called the Energiewende. Some current projects include: (1) E.ON's 2 MW Power-to-Gas unit powered by wind energy, was installed in Flakenhagen, where they injected H_2 into the existing gas system for the first time in 2013 [29]; (2) Audi's e-gas plant has been in operation since 2013 in Werlte (Germany) and it is the world's largest P2G plant (6MW) [30]; (3) Hydrogenics recently awarded a 2.4 MW Power-to-Gas plant in Germany, that will be connected to the local NG

pipeline and powered by wind energy [31]. While such installations are significant, P2G is a relatively new concept that has not been as thoroughly explored as other storage technologies, i.e. most of the P2G pilot plants have only been operated for a short time as stand-alone systems, and few have operated for long-term [9]. Despite setting rigorous renewable energy goals in several North American regions, the P2G concept has not received as much recognition or adoption in North America as in Europe, although Canada is initiating one project in Ontario [33] and the first P2G demonstration site in the United States is taking place at the University of California, Irvine campus [34].

Finally, by connecting the power sector to the gas grid, P2G has the transformative power to change how renewables are integrated: (1) enabling massive energy storage, (2) enabling seasonal storage, (3) cost-effectively delivering energy by use of existing ubiquitous gas infrastructure, and (4) making energy delivery more resilient with both gas and electric infrastructure.

These benefits of the P2G concept will be achieved only when the challenges related to the containment of H_2 in the NG system can be overcome. The challenges to further development of P2G include distribution and storage of H_2, pipeline embrittlement and fatigue crack growth enhancement, and the unique features of H_2 (flammability limits, diffusivity, density) which are very different than current ubiquitous fuels [35]. Of particular interest here is the propensity of H_2 to leak from existing gas infrastructure. Intuition associated with H_2 molecule size and high diffusivity together with previous research [36]–[38] suggests that H_2 will be more difficult to contain and will leak much more quickly than NG in the same infrastructure. H_2 and NG leakage in the low-pressure

infrastructure of the NG distribution system, downstream of the customer meter are the particular focus of the current work.

2.2 Challenges of Introducing H_2 to NG infrastructure

H_2, the immediate gaseous fuel that is produced from P2G, is a multifunctional fuel and is viewed as a promising energy carrier for the future due to its ability to mitigate air pollution, provide sustainable automotive transportation, and provide security of energy supply [39]. Production of H_2 by electrolysis from water and renewable power with zero emissions, followed by storage, and followed by conversion in a fuel cell back to electricity and water is a completely sustainable and renewable cycle that society could depend upon in perpetuity. H_2 has many proposed pathways and end uses including: (1) direct injection in the NG grid at low concentrations to ensure a grid-compatible gas mixture for all current gas end-uses; (2) immediate storage in pressure tanks for applications that require pure H_2; (3) conversion of H_2 to methane (CH_4) using captured CO_2, where CH_4 can be subsequently fed into the NG grid, as renewable CH_4, in unlimited quantities [28]; (4) Electricity conversion with fuel cells or internal combustion engines [13]; (5) use to produce ammonia, cement, or other chemicals [16], and (6) use as a fuel in difficult-to-electrify transportation applications that require rapid fueling, long range or large payload [40].

Direct injection of renewable H_2 into the NG grid would result in the most environmental and thermodynamic benefits for the P2G process since H_2 is a clean energy carrier and the immediate product of P2G. H_2 has the transformative power to advance how renewable fuels and renewable energy conversion systems are integrated with existing infrastructure by connecting the power sector to the NG grid. Although the role of

H_2 as a sustainable energy carrier has been foreseen as increasingly important, there is a lack of quantitative work that analyzes the degree to which gaseous fuel leakage may be enhanced in the NG system by the addition of H_2, particularly in the low-pressure distribution parts of the system [41]. Limited information exists regarding the H_2 tolerance of NG infrastructure and its components and some information is contradictory [13]. Even fewer studies assess the potential impact on end-use components of the NG system since end-use requirements are typically the strictest for increasing H_2 blend levels [37]. Limited studies report the impacts of introducing H_2 to low pressure, residential NG infrastructure. Many of the published studies about H_2 limits on NG infrastructure are in German (i.e. see [42], references 125 and 126 from [13]).

2.2.1 The NG System

NG is an important source of energy for the United States; in 2017, NG made up 29% of the total energy consumed in the country [43]. NG is a mixture of combustible gases and it is mostly composed of methane (CH_4) with trace amounts of ethane, propane, and other hydrocarbons. The volumetric fraction of methane may vary from region to region, but it is typically over 90% by volume.

The NG system is a "highly integrated network" with over three million miles of pipelines in the US, which transport NG from the source to and from storage facilities and to consumers [44]. A map of major pipelines in the United States is shown in Figure 3. The NG system is comprised of wellheads, processing plants, compressor stations, storage facilitates, distribution centers, and metering stations. Each component has its own variety of pipelines, controllers, valves, and fittings [44]. Further, the NG system serves various sectors, including the industrial, electrical power, residential, commercial, and

transportation sectors. The major applications for NG include heating for households, commercial businesses, centralized power generation in gas turbines, and decentralized combined heat and power plants [28]. A schematic of NG production and delivery is shown in Figure 4.

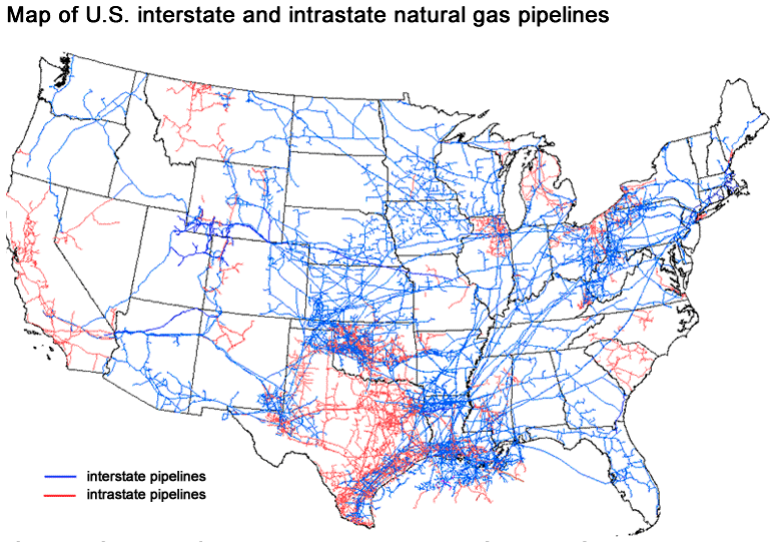

Figure 3: NG piping network in the continental U.S (from [44])

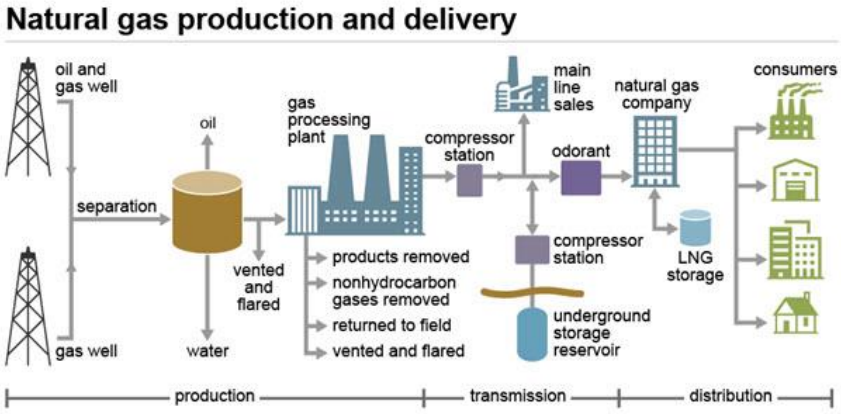

Figure 4: The NG system is a complicated network that delivers NG from many sources to a wide variety of consumers (from [45])

Injection of H_2 into the NG system is an attractive method of transporting and storing H_2, since the NG system has potential to connect renewably produced H_2 with an already-

established market [28]. This includes the industrial, commercial, residential, transportation, and electric power sectors (see Figure 5). If H_2 is injected into the NG grid, however, it has potential to impact all of the infrastructure that delivers NG to these sectors in addition to the diverse population of installed appliances [46]. The residential and commercial sectors are especially impacted due to differences in combustion performance characteristics such as the Wobbe index (see

Table 1 below). Significantly, much of the previous research on H_2 impacts to NG infrastructure has focused on assessing the safety and performance of various end-use appliances. Safety aspects are assessed by quantifying the risk of flashback [46], while the performance of the appliance is assessed by analyzing changes in the Wobbe index, or measure of the fuel thermal input that would flow through any given orifice size of the gas end-use (e.g., appliance).

Flashback is an important parameter for evaluating the safety of combustion devices on the consumer-side of the meter, since it can cause flame extinction which can lead to appliance shut down, damage to the burner, and it poses a safety hazard since it could lead to leakage of combustible mixtures in homes or enclosed areas [46]. Flashback occurs when the burning velocity exceeds the velocity of the unburned mixture destabilizing the flame, and potentially causing the flame to "flack back" from the burner and upstream into the appliance [46]. The risk of flashback is higher for H_2 than for NG in fuel-rich flames because H_2 has a laminar flame speed that is 5 times higher than methane and operating fuel concentration of burner heads are often within the range of H_2's broad flammability

limit (from 4 - 75%) [47]. In order to prevent flashback from occurring, previous studies have suggested limits of less than 20% H_2 addition [47].

Additionally, the Wobbe index represents the thermal input to an appliance and it is the ratio of the higher heating value to the square root of the specific gravity. It has been widely used since the 1920s as a parameter than can effectively evaluate the interchangeability of various fuels [47]. The Wobbe Index assumes incompressible and inviscid flow at steady state and with negligible pressure loss and these assumptions are valid for appliances [47]. The Wobbe Index plays a central role in comparing gaseous fuel mixtures since it is indicative of the effect of gas composition changes on the heat input at a constant pressure to a domestic appliance [48]. Two fuels with the same Wobbe Index will have the same heat output for the same appliance if the inlet pressure is constant [47]. Since the Wobbe index of H_2 and CH_4 is similar, a portion of the CH_4 in NG can be replaced by H_2 at low concentrations without significantly altering the performance of combustion devices [47]. However, significant addition of H_2 to NG will decrease the Wobbe Index of the fuel. It will be important to consider the regional Wobbe index of NG before H_2 is added to ensure that the performance of the combustion device is not impacted because gas composition varies regionally, even within a country [46].

Further, the residential and commercial sectors, which use NG to heat buildings, heat water, to cook, and to dry clothes, for example, may have the strictest requirements for increasing H_2 blend levels in the NG system. Studies such as those reported by NREL indicate that end-use requirements are typically the strictest for increasing H_2 blend levels [37]. Combined, the residential and commercial sectors make up 28% of the total NG consumed in the US [49]. The complexity, size, and connected nature of the NG distribution

system makes it challenging to assess how gaseous H_2 fuel may affect the existing NG system. Finally since the composition of NG may vary from region to region, it may further complicate assessment of the impacts of H_2.

$$\text{Wobbe Index} = \frac{\text{Higher Heating Value}}{\sqrt{\text{Fuel Specifc Gravity}}} \quad (1)$$

Table 1: Characteristics of H_2 and CH_4 that may impact the combustion performance of appliances from [46]

Parameter	CH_4	H_2	Ratio (CH_4/H_2)
Higher Heating Value (MJ/m^3)	39.82	12.75	3.1
Relative density	0.555	0.070	7.9
Wobbe Index (MJ/m^3)	53.45	48.34	1.1
Number of Oxygen molecules needed for complete combustion of 1 fuel molecule	2	0.5	4
Number of air molecules needed for complete combustion of 1 fuel molecule	9.5484	2.3871	4
Burning Velocity (cm/s)	36.7	203.9	0.180
Adiabatic Flame Temperature (K)	2226	2381	0.935

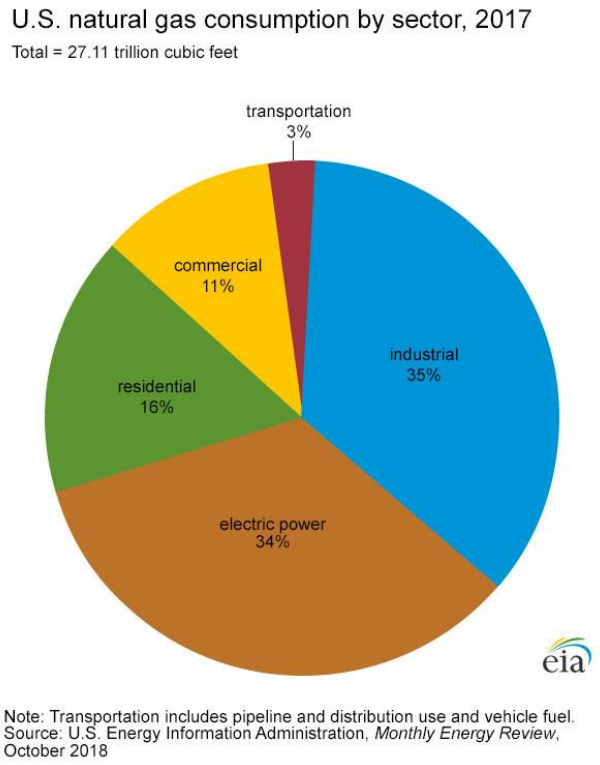

Figure 5: NG consumption by sector in the U.S (from [50])

2.2.2 H_2 Impacts on Residential Infrastructure

Studies have suggested that relatively low concentrations (less than 5% and up to 15% by volume) of H_2 in the NG system appear to be a viable option that may not significantly increase the risk of introducing such a blend to the overall public safety or the durability and integrity of the existing NG infrastructure [37]. However, because of H_2's unique physical characteristics (e.g., high diffusivity, low molecular weight, low viscosity, lower volumetric heating value, and propensity for pipeline materials embrittlement), direct injection of H_2 into the NG system has raised concerns over have raised concerns regarding safety aspects of transmission, distribution, pipeline durability, pipeline integrity, end user appliances' performance [51], and leakage. The maximum allowable H_2

concentration will depend on the limits of individual components, like compressors, and applications, such as end-users and will vary depending on the region, country and applications [28].

Currently, some NG distribution systems permit varied quantities of H_2 to be present in the NG system. In Hawaii, manufactured gas is delivered with significant H_2 blends and these gas mixtures are used for heating and lighting applications [37]. Additionally, in the European Union, allowable H_2 concentrations vary for each country, ranging from 0 to 12%vol [52]. In [53], Altfeld and Pinchbeck found that an admixture of up to 10% vol of H_2 is possible in some parts of the NG system. Though they claim it is not possible to identify a H_2 limit that would apply for all parts of the European gas infrastructure, they found some components may not be adversely affected by the addition of a 10% H_2 admixture [53]. They found leakage from transmission pipelines and compressors and metering and billing equipment was negligible when H_2 was introduced [53]. The safety parameters of in-house pipework systems and industrial applications were only affected marginally by 10%vol H_2 blends [53]. The authors recommend further research on specific gas burners to gain more insights on domestic applications.

NREL published a report on the key issues regarding H_2 injections in the NG system from studies conducted by the Gas Technology Institute, International Energy Agency, and the Naturally project, associated with the European Commission [37]. They found that conditions that determine an allowable H_2 injection limit vary significantly depending on the composition of NG, the type of appliance, and age of the appliance; acceptable ranges range between 5% and 20% H_2 [37]. They also report that the literature may overestimate the gas that is lost in systems containing low concentrations of H_2 at low pressures (e.g.,

3psig or 0.25 psig). Additionally, H_2 will permeate 4 to 5 times faster in the plastic pipes typically used in distribution lines [37].

Recent studies have focused on the potential impacts of H_2/NG mixtures on the performance of residential appliances. In [46], De Vries et al. develop a computational interchangeability analysis for determining the possible impacts of H_2 addition on domestic appliances. The authors describe that two gases are interchangeable if substitution of one gas for another does not lead to significant deterioration in the performance of a given appliance; the performance of the system can be subdivided in aspects for safety and fitness for purpose [46]. Due to the variety of the population of domestic appliances and NG composition, their approach is based on fuel composition using fundamental combustion parameters. Further, a similar interchangeability approach is needed to assess all possible impacts on gaseous fuel leakage. Additionally, Choudhury et al. investigated the influence of 5% H_2 in NG and 10% CO_2 in NG on the water heaters [54]. In the study, the author observed that both the low-NOx and conventional water heaters operate safely when mixtures of 5% H_2 in NG and 10% CO_2 in NG are introduced [54]. In [47], Zhao et al. use a representative cooktop burner to study the influence of H_2 addition on the performance of the appliance. The experimental results suggest the burner is able to safely operate without modifications with blends up to 15% H_2 by volume.

Understanding and mitigating H_2 leakage from the NG system is important to understand how gaseous H_2 fuel may impact NG infrastructure. To understand H_2 leakage there is a need for quantitative analyses which accurately characterize the physical mechanisms of leakage, leakage rate, and the degree to which leakage may be enhanced when H_2 is introduced to the NG system. Current understanding of the maximum H_2

concentration allowed in the NG system is not definitive; and methods to assess the impact of H_2 on leakage are not consistent. Gaseous fuel leakage that occurs on the customer-side of the meter has not been as thoroughly studied as gaseous fuel leakage in utility infrastructure. More research is needed to assess gaseous fuel leakage at pressures closer to the actual operating pressures of distribution lines and at concentrations that are closer to actual desired concentrations [37].

2.3 Overview of Gaseous Fuel Leakage

Since the beginning of gaseous fuel leakage research pertaining to H_2 and methane (CH_4), the main component of NG, the consensus among researchers has been that H_2 should leak between 1.3 to 3 times faster than methane due to the differences in chemical and molecular properties (e.g., density, viscosity, and diffusivity, etc.) between these two gaseous fuels in various leakage flow regimes (e.g., see [36]–[38], [51]). Current experimental results and a close observation at a previous study about H_2 leakage from real-world, practical NG fittings suggests that classical fluid dynamics theories used to predict gaseous fuel leakage may not be applicable for predicting leakage rates of H_2 and NG from certain practical leaks such as those that are typical in low pressure NG infrastructure. In the following subsections, various fluid flow theories and related studies pertaining to gaseous fuel leakage are presented. An analysis of the theory that the authors suggest is most relevant for gaseous leaks from typical low-pressure NG infrastructure, based upon our results, is presented in Section 0.

2.4 Classical Gaseous Fuel Leakage Theories

Nearly all of the literature has assumed classical fluid mechanics theories can be used to model gaseous flow leakage from NG infrastructure. The classical model is represented by

use of the Navier-Stokes equations and characterizes fluid flows with spatial and temporal variations of density, velocity, pressure, temperature and other macroscopic flow quantities [55]. The continuum approximation assumes a flow is comprised of matter that is fully continuous and indefinitely divisible, while ignoring the molecular nature of fluid particles [55]. Additionally, at the macroscopic scale, it is assumed that the size of the channel is many times larger than the mean free path of the molecules so that the majority of molecular collisions occur between molecules; this allows the flow to be assumed in thermodynamic equilibrium so that the frequency of intermolecular collisions is high enough that the collisions between the molecules and the wall boundaries can be ignored [56]. Most classical fluid theories for analyzing macroscopic systems assume internal flows are continuous, fully developed, incompressible, have a constant viscosity, and have no-slip boundary conditions. Fully developed flow is a flow for which the radial velocity distribution is independent of the axial flow direction and it typically occurs at a distance that is significantly far from the inlet [57].

Finally, the no-slip boundary assumption refers to the assumption that the fluid has a velocity equal to zero at the boundaries (e.g., walls of the channel, passage, or pipe), or the same velocity as the boundary if the boundary is moving [58]. The classical model is sufficiently accurate as long as local properties such as density and velocity can be defined as averages and the flow is in thermodynamic equilibrium [56]. The basis of the no slip boundary condition is that the collisions between the boundary wall and the fluid particles are infinitely high so that there are no discontinuities of velocity within the fluid, otherwise, there would be infinite velocity gradients [55]. The no slip boundary assumption is valid only if the “flow adjacent to the surface” is in thermodynamic equilibrium [55].

The consensus among most of the gaseous fuel leakage literature has been that the main modes of gaseous fuel leakage from NG infrastructure are leaks driven by convection or by diffusion that can be characterized using the classical fluid flow theories. Leaks driven by pressure gradients (convection) such as flows through “holes, breaks, and defects in the material surfaces” may occur as either subsonic laminar or turbulent flow, or as choked flow [38]. These leaks are typically at subsonic pressures, especially for leaks through fittings and infrastructure in a residential setting due to the low-pressure or such infrastructure.

The literature has assumed that the convection-driven leaks will occur in the continuum viscous flow regime assuming the aperture is much greater than the mean free path [38]. If this is the case, then the leaks will either be governed by laminar or turbulent convection physics and can be analyzed using traditional fluid mechanics theories. In addition to subsonic laminar and turbulent flows, leakage of gases may also occur as permeation or diffusion of gases. Diffusion is driven by a concentration gradient, which could occur under circumstances of gas separation within the infrastructure or conditions of very low- pressure difference with large concentration differences along the length of the leakage path. The mathematical equations and analyses used to describe these types of leaks are presented in the following sections:

1. To characterize low-Reynolds number pressure convection-driven leaks, various authors ([36], [38]) have proposed the Hagen-Poiseuille equation for laminar flow:

$$Q = \frac{\Delta P \pi D^4}{128 L \mu} \quad (2)$$

Where ΔP is the pressure drop across the leak, D is the diameter of the leak, L is the length of the leak, and μ is the dynamic viscosity. By this theory of laminar flow H_2 should leak faster than CH_4 for the same leak hole geometry, pressure drop and surface roughness, in inverse proportion to the ratio of the viscosities of H_2 and CH_4. Since the viscosity of H_2 is typically 1.29 times lower than that of CH_4, H_2 should leak 1.29 times faster than CH_4 in this flow regime.

2. Similarly, for high-Reynolds number pressure convection-driven leaks in the turbulent regime, these authors have both proposed that a constant friction factor be used in the Darcy Weisbach equation as follows:

$$Q = \frac{0.354 * \sqrt{\Delta P} \pi D^{2.5}}{\sqrt{f L \rho}} \quad (3)$$

Where f is the friction factor, and ρ is the density. Now, the ratio of the leak rate between H_2 and CH_4 for the same leak hole geometry, pressure drop and surface roughness, is equivalent to the inverse square root of ratio of the density of H_2 to CH_4. Since the density of H_2 is 7.96 times lower than that of CH_4, H_2 should leak 2.82 times faster than CH_4 in this flow regime.

3. Finally, for leaks involving diffusive mass transport, [36] proposes Fick's law of diffusion as the governing equation of transport as follows:

$$Q = A(-D\frac{\partial c}{\partial x}) \quad (4)$$

Where Q is molar flowrate, A is cross sectional area of the leak, D is the diffusion constant of the gas, and $\frac{\partial c}{\partial x}$ is the concentration gradient. Using this equation for diffusion, the ratio of the flow rates of H_2 and CH_4 is equivalent to the ratio of the diffusion coefficients of these gases. Since the diffusivity of H_2 is typically 3.15 times higher than that of CH_4, H_2 should leak 3.15 times faster than CH_4 in this flow regime.

While in [38], Schefer et al. propose a combination of Fick's first law and Sievert's law to approximate the diffusion rate of gases through a metal as follows:

$$J = \frac{DS\sqrt{P}}{l} \quad (5)$$

Where J is the permeation rate (mol s^{-1} m^{-2}), D is the diffusivity constant, S is the solubility (Sievert's Parameter), P is the pressure, and l is the length of the passage.

Additionally, Ge and Sutton [59] propose three potential leakage modes to investigate H_2 leakage through threaded fittings: (1) Permeation, which occurs when there is no gap between screw surfaces; (2) When there is a constant gap between mated screws, the gas will flow through the spiral grooves due to pressure gradients; (3) If a "certain length of mated screw contacts well, while the rest of the length of the mated screw has a constant

gap between opposite surfaces" then the mass transfer of H_2 will be due to diffusion through the solid, and to convection through the micro spiral grooves [59]. Figure 6 is a representative image of a fitting and Figure 7 represents the various modes of leakage described by Ge and Sutton.

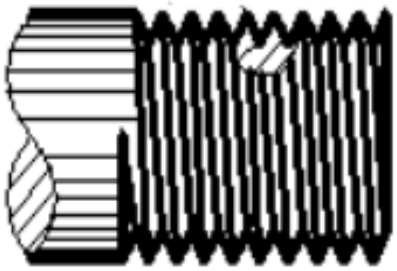

Figure 6: Mated screw connection fitting from Ge and Sutton [59]

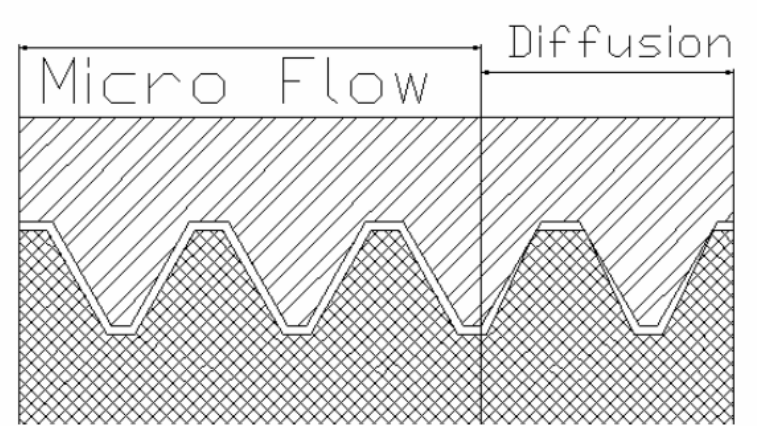

Figure 7: Various modes of leakage through mated screw connections (from [59])

Rather than analyzing the flows using conventional fluid theory in the continuum regime, Ge and Sutton propose that leaks which occur between the screw gap of National Pipe Thread (NPT) fittings or between the microchannels in contacting surfaces should be modelled in the slip flow regime. If the channel height, represented by the screw gap between the male and female threads, is small enough, the Knudsen number will increase

to a value greater than 0.01 and the rarefaction effects cannot be ignored [59]. Additionally, Ge and Sutton derive analytical models to predict the leakage of H_2 through fittings using the slip boundary condition, various molecular models, mean free path, tangential momentum, and the 2-D compressible Navier-Stokes equations. They also construct an experimental apparatus using ¼ NPT fittings and ⅜ NPT fittings to compare the predicted mass flow rate vs pressure ratio of the analytical model versus experimental results.

The analytical models, developed by Ge and Sutton, predict the leakage flowrates using Knudsen number calculations based on the Hard Sphere Molecular model and the Maxwell Molecular model. They assume the leaks will occur in the slip flow regime with negligible permeation. The findings of Ge and Sutton in [59] only yield a converged solution between the analytical models and experimental results for the ¼ NPT fittings but not for the ⅜ NPT fitting. The authors state that due to "the complexity of the leakage modes" and the significance of permeation, a converged solution was not achieved for the ⅜ NPT fitting experiments [59]. It is likely that for the ⅜ NPT fitting, variations in the leak path dimensions led to variations in flow regime that were not all accurately characterized in the analytical model which only included assumptions for the slip flow regime. For the ¼ NPT fitting results, the Knudsen number calculations differ by 0.03 between the Maxwell and Hard Sphere molecular models, both of the Knudsen numbers suggest the flow is in the slip flow regime. Additionally, the authors predict that thread surface roughness is likely to increase the effect of diffuse reflection of the gas molecules, especially for H_2. They conclude that all fittings leak even a minute amount of gas.

In [60] Qi et al. develop a nonequilibrium molecular dynamics simulation to investigate the mechanism of helium gaseous leakage through a clearance seal. Since computational

fluid dynamics methods assume steady, laminar, incompressible flow with constant viscosity, CFD is not applicable for these types of micro-sized flows [60]. They observe that the leakage mechanism occurs mainly through the diffusive motions of the atoms through adsorption layers near the walls and they find that the density in the channel of the leak is not constant; most of the atoms are accumulated in the adsorption layers instead of the central region. It is possible that in a practical leak, similar characteristics can be observed as those presented in Qi et. al.'s study. In a practical leak, it is possible that the density of the escaping molecules may not be constant throughout the leak area because (1) the mechanism of the gas escaping through the leak may occur carried out layer by layer and (2) the density of the gas source might be much greater than the density of the leak gas. Thus, this work provides an additional theory that may explain observations of leakage that do not comply with continuum theories of leakage flow.

Although some of the literature uses computational fluid dynamics (CFD) to simulate leaks, this approach may not be necessarily appropriate to analyze leaks through threaded fittings in existing systems. CFD methods assume conditions of steady laminar flow, incompressible, constant temperature and constant viscosity [60]. In real low-pressure NG piping systems with steel or iron pipes, it is very likely that gaseous fuel leakage will primarily occur through the threads or mechanical joints of the piping systems such as connections between pipes and elbows, tees, unions, and caps rather than through the metallic surfaces of pipes- similar to what Ge and Sutton describe in [59]. The majority of the leaks encountered in threaded fittings may be described as "labyrinth type leaks" with "long, narrow, cracks [51]." The tortuous path that characterizes the exit length of a leak may induce a pressure drop governed by friction, surface roughness, and diffuse reflection

of molecules which may affect the development of the velocity profile and may affect compressibility.

Thus, the majority of gaseous fuel leakage will occur through passages created by misalignments and/or defects amongst the mated screws. While the authors of [59] derive an analytical model of the leakage through a fitting as a microchannel with a constant height, in a real fitting the connection between the mated screws will not be constant and will be much more tortuous than a rectangular duct. The channel height might vary significantly throughout the path of the leak thus disrupting continuous flow.

The limited experimental research so far has made it largely uncertain whether the traditional fluid mechanics theories can accurately characterize leakage from such NG infrastructure.

2.5 Discrepancies in Literature about Gaseous Fuel Leakage

Findings from the seminal Swain and Swain study "A Comparison of H_2, CH_4, C_3H_8 Fuel Leakage in Residential Settings" [36], suggest that in real world fitting leak circumstances, H_2, CH_4, C_3H_8 will leak at the same or similar rates for most leaks. The authors attribute these results of similar leak rates for H_2 and other gases to "entrance effects." [36] Though this paper has been widely referenced in the field of gaseous fuel leakage, no other study has repeated nor acknowledged their significant findings that suggest H_2, CH_4, and C_3H_8 will leak at the same or similar rates in real fittings.

In [36], Swain and Swain use representative fittings with leaks to experimentally determine the leakage flow regime and flow rate for various gaseous fuels. Figures 4 through 11 of the study demonstrate a log-log plot of the pressure drop across a leak vs volumetric flow rate for H_2, CH_4, and C_3H_8 in eight different faulty fittings that represent

real fittings from residential piping systems. Since the authors find most of the leaks to remain in the laminar flow regime, they claim that H_2 "leaks will produce lower volumetric flow rates than what has been predicted in the literature." Experimentally, they find H_2 leaked an average of 1.55 times faster than CH_4. This value includes the effect of the elevated line pressure required for an equivalent energy delivery rate with H_2.

However, upon a closer look at Figures 4 through 11 of the Swain and Swain study, for most of the leaks at pressures lower than 4 kPa, the pressure and corresponding flow rate between H_2 and CH_4 is nearly identical. In other words, significant overlap in the leakage rate plots of H_2, CH_4, and C_3H_8 is observed. This overlap is particularly noticeable in Figures 4, 5, 10 and 11, where the overlap exceeds 4kPa and extends to higher pressures. Some examples of the results of Swain and Swain that shows this effect are reproduced in Figure 8.

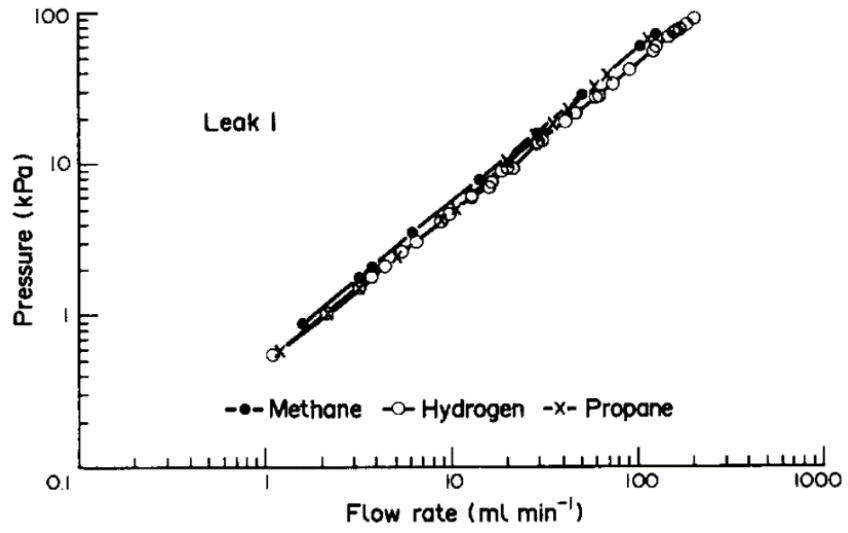
Leak 1
Pressure (kPa)
100
10
1
0.1
Methane
Hydrogen
Propane
1
10
100
1000
Flow rate (ml min^{-1})

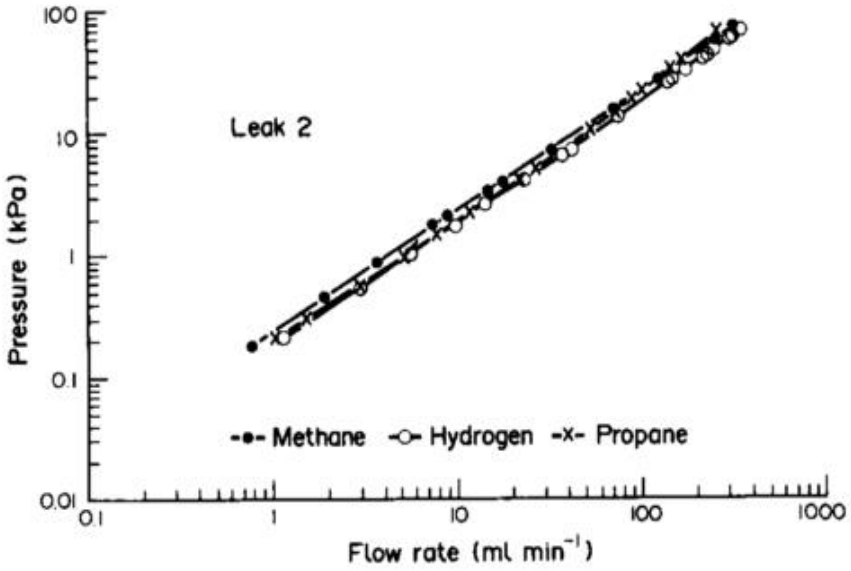
Leak 2
Pressure (kPa)
100
10
1
0.1
0.01
Methane
Hydrogen
Propane
0.1
1
10
100
1000
Flow rate (ml min^{-1})

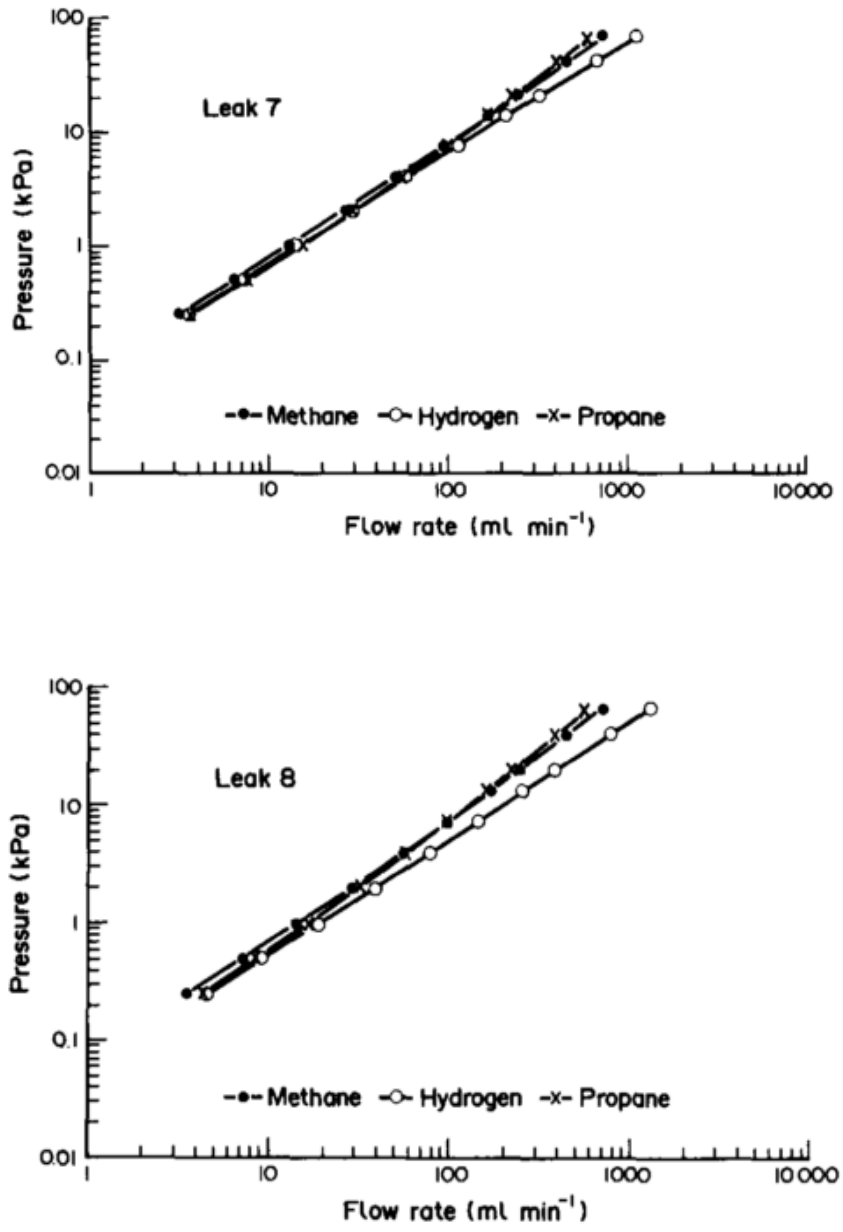

Figure 8: Selected figures from [36] which show the pressure drop vs flow rate for various representative fittings.

Notice that the pressure drop appears to be nearly the same for all gasses throughout various ranges of flow rates and fittings tested. These results suggest the leakage of H_2, CH_4, and C_3H_8 through these fittings is nearly the same under these low-pressure conditions, particularly for Leak 1 and Leak 2. Additionally, for Leak 7 and Leak 8, the flow rates

appear identical for NG and H_2 for a range of pressures. To explain this observation, the authors attribute these findings to the "onset of significant entrance effects" and do not further mention these similarities in the paper or in any of the gaseous fuel leakage research literature that follows this widely cited study, despite these impactful results which suggest that in many real-world fittings, H_2, CH_4, and C_3H_8 may leak at the same or similar rates for certain types of common, practical leaks. In typical NG piping systems in the residential sector NG is contained at low pressures in the range of 4-12 inH_2O gage (~1-3 kPa) (e.g., see [61]–[63]). When this is considered in relationship to the results from [6], it appears that minimal to no difference in leakage should be expected for gaseous fuel blends of H_2, CH_4, and C_3H_8 in residential piping systems. Further, the rest of the literature about gaseous fuel leakage from NG infrastructure assumes gaseous fuel leaks through NG fittings and infrastructure can be described as fully developed, either laminar or turbulent, incompressible, inviscid, and steady.

Despite the results from the seminal study of Swain and Swain in 1992 which suggest many of the leaks in residential fittings will occur through flows that are not fully developed [36], no studies have investigated the possibility of a leak with flow that is not fully developed. If the flow velocity profiles are not fully developed, then the traditional properties used to predict flow rate (such as density, viscosity, molecular weight) may not apply to such flows. Flow compressibility affects both the velocity profile and friction factor [64] . Previous studies have suggested that a fluid flow can never be fully developed dynamically and thermally when the flow through small cross-sectional areas is compressible [64]. Finally, even though Swain and Swain attribute their interesting

findings to entrance effects, all the subsequent literature about gaseous fuel leakage does not mention entrance effects and assumes H_2 should leak much faster than CH_4.

2.6 Overview of Gas Flow Theories

Since the beginning of gaseous fuel leakage research pertaining to H_2 and methane (CH_4), the main component of NG, the consensus among researchers has been that H_2 would leak between 1.29 and 3 times faster than methane due to the differences in density, viscosity, and diffusivity between these two gaseous fuels. Current experimental results and a close observation at a previous study about H_2 leakage from real-world, practical NG fittings suggests that classical fluid dynamics theories used to predict gaseous fuel leakage may not be applicable for predicting leakage rates of H_2 and NG from certain practical leaks such as those from NG fittings.

In the following subsections, various fluid flow theories pertaining to gaseous fuel leakage are presented. An analysis of the theory that may best explain the results in this thesis is discussed in Section 6.

2.6.1 Classical fluid Mechanics Theories

Most of the literature uses classical fluid mechanics theories based upon the continuum approximation to model leaks through fittings as macroscopic internal flows. In classical fluid mechanics, internal flows are typically modelled as fully continuous, indefinitely divisible, fully developed, incompressible flow with no-slip boundaries. Internal flows require special considerations; since the fluid is in constant contact with the surface, it is especially important to consider the viscous effects and the development of the hydrodynamic boundary layer for internal flows. As the fluid moves further away from the entrance region, the inviscid flow region shrinks and the boundary layer merges in the

center of the cross section of the conduit [65]. This is shown in Figure 9 for a laminar flow. Once the boundary layer has merged, the viscous effects are significant over the entire cross section and the velocity profile is no longer changing along the path of the fluid. When the velocity profile is constant, the flow is considered to be fully developed.

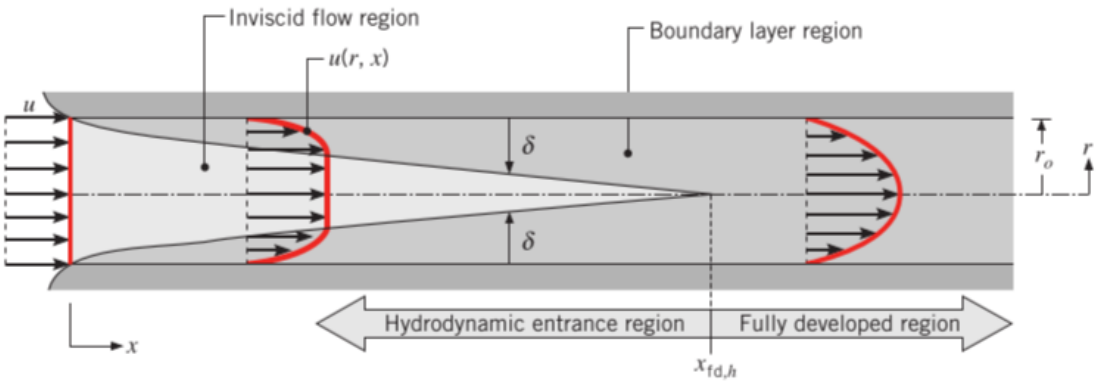

Figure 9: Hydrodynamic boundary layer development in a circular tube for laminar flow (from [65])

The flow regime, determined by the dimensionless Reynolds number, is also important to consider for internal flows. The Reynolds number is a ratio of the viscous to inertial forces. For a fluid flowing through a conduit with a circular cross section, it is given by

$$Re_D = \frac{\rho v d}{\mu} \tag{6}$$

where ρ is density, v is velocity, d is diameter, and μ is dynamic viscosity. If the flow is fully developed, the bulk flow can be categorized as either laminar, turbulent, or transition flow from the Reynolds number. Below a critical Reynolds number, the flow will be laminar and above the critical value the flow will begin a transition to turbulence. The transition to turbulent flows from laminar will be influenced by viscoelastic properties. The flow regime

determines the hydrodynamic entrance length and the development of the velocity profile. The velocity boundary layer development is shown in Figure 10.

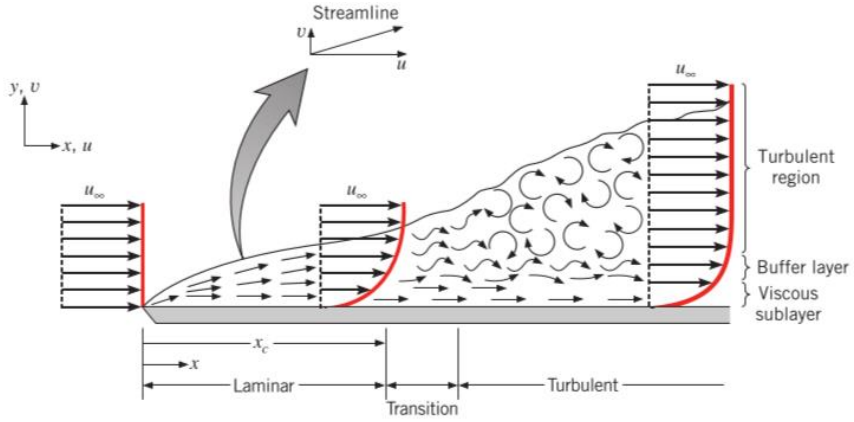

Figure 10: Velocity boundary layer development (from [65])

For a laminar flow through a conduit, the Reynold's number must be less than 2300 and the velocity profile will be parabolic. Laminar flows have smooth streamlines and if the fluid velocities vary, they will vary smoothly with position and time [58].

For laminar flow, the hydrodynamic entrance length, $x_{fd,h}$, can be estimated from

$$\left(\frac{x_{fd,h}}{D}\right)_{lam} \approx 0.05 Re_D \tag{7}$$

assuming the fluid enters the tube from a rounded converging nozzle and is characterized by a nearly uniform velocity profile at the entrance [65].

For turbulent flows, much larger Reynolds numbers are needed to achieve conditions that are fully turbulent, Re ≈ 10,000. Turbulent flows can be characterized as flows with chaotic velocity fluctuations in time and space [58]. There is no satisfactory equation to describe the entrance length for flows that are fully turbulent, however, it is thought to be independent of the Reynolds number. Thus, from [65] as a first approximation:

$$10 \leq \left(\frac{x_{fd,h}}{D}\right)_{turb} \leq 60 \tag{8}$$

In classical fluid mechanics, the Navier Stokes equation, derived from Newton's second law of motion in differential form, is used most often to describe flows through channels. The Navier Stokes equation is a momentum balance of the flow. For a Newtonian fluid in a smooth, circular pipe of constant diameter with axial symmetry, and laminar flow that is steady, incompressible, and with constant viscosity, the solution of the Navier-Stokes equations corresponds to the Hagen-Poiseuille equation [58]:

$$Q = \frac{\pi \Delta P D^4}{128 \mu L} \tag{9}$$

where, P is pressure, D is diameter, μ is dynamic viscosity, and L is length. This equation assumes flows will occur in the continuum regime through a channel with a parabolic velocity profile that is fully-developed and no-slip conditions at the boundaries. Under these assumptions, the relationship between flowrate, Q, and Pressure drop, is linear for laminar flows. The Hagen-Poiseuille equation is the equation that is most often used to describe gaseous fuel leakage through NG fittings (See [36], [38] and Section 2.4). Note, that for laminar pipe flows, the effect of surface roughness is negligible. Finally, the Fanning Friction factor, f, is a dimensionless variable that is used to relate the frictional pressure drop per unit length to pipe diameter, density, and average velocity. It is used for both laminar and turbulent flows. The Fanning friction factor, f, is given by [58]:

$$f = \frac{D \Delta P}{2 \rho L V^2} \tag{10}$$

Where D is diameter, P is pressure drop, ρ is density, L is length, V is velocity. For laminar flows, the Fanning Fricion factor is only a fucntion of the Reynolds number [58]:

$$f = \frac{16}{Re} \tag{11}$$

The fluctuating nature of turbulent flows leads significantly influences the stability of the fluid and flow variables which vary with time. Turbulent flow is less ordered than laminar and is comprised of eddies which results in lateral mixing, making it susceptible to be affected by even the smallest disturbances. Unlike laminar flow, turbulent flow is strongly affected by surface roughness. Thus, the analytical solution to describe turbulent flows is much more complicated in comparison to the solution for laminar flow [66]. For turbulent flows, the Fanning Friction factor is a necessary consideration to relate pressure drop and flowrate. For turbulent flows in smooth pipes [58]:

$$f = \frac{0.079}{Re^{0.25}} \tag{12}$$

This equation is valid for 4,000 < Re < 10^5 and is based on the Blasius equation [58]. Thus, for a smooth pipe, the friction factor is only a function of the Reynolds number. The Fanning friction factor then can be related to the flow rate using the relationship between velocity, area and flowrate [67]:

$$Q = A * V = \frac{\pi D^2}{4} V \tag{13}$$

$$\Delta P \sim L\, \rho^{3/4} \mu^{1/4} d^{-4.75} Q^{1.75} \tag{14}$$

Thus, for turbulent flow through a smooth pipe, the pressure drop is proportional to nearly the square of flowrate. For turbulent flow, the pressure drop is only slightly affected by viscosity. Note, this is a characteristic of turbulent flow [67].

For a rough pipe, the relative roughness ϵ/D affects the friction factors and must be included in the calculation. Thus, for a rough pipe [58]:

$$\frac{1}{\sqrt{f}} = -4\,log\left[\frac{\epsilon}{3.7D} + \frac{1.256}{Re\sqrt{f}}\right] \quad (15)$$

For a given roughness, the friction facotor will become constant (fully rough) at very high Reynolds numbers and thus, independent of the Reynolds number [67], so that

$$\frac{1}{\sqrt{f}} = -4\,log\left[\frac{\epsilon}{3.7D}\right] \quad (16)$$

This equation is applicable to a completely turbulent flow regime.

2.6.2 Modeling flows through Microchannels

Two fundamental methods are used to model a flow field: (1) modelling the fluid as a collection of molecules; (2) modeling the fluid as a continuum of matter [55]. Deterministic and probabilistic methods can be used in the first method to model the fluid as a collection of molecules and nonlinear partial differential equations are used in continuum models [55]. Fluid modelling methods are shown schematically in Figure 11.

It is likely that gaseous fuel leaks from existing NG NPT fittings may occur through gaps that are much smaller than could be modeled by theories previously presented in the literature. When dealing with such gaseous fluid flows, depending upon the size, shape, and microstructure of the channel and the characteristics of the diffusing gas species, it is likely that wall effects and other molecular dynamics cannot be neglected or assumed to be in equilibrium. As the size of the channel approaches the mean free path of the molecules, the continuum assumption becomes invalid and the flow begins to depart from equilibrium. The linear relationships between stress and rate of strain and between heat flux and temperature gradient, and the no-slip velocity boundary conditions also become invalid because the gas molecules at the boundary have a velocity and temperature that is not equal to the velocity and temperature of the boundary [55]. As the size of the flow channel

is reduced, the interactions between the molecules and the wall boundaries become more significant and possibly even more frequent than intermolecular interactions. In fact, initial deviations from the continuum model first appear with respect to the boundary layer [68]. The first sources of thermodynamic disequilibria appear at the wall because there are fewer intermolecular gas interactions and more interactions with the wall boundary surface.

Surface effects become especially important to consider in flows through small channels, as the surface-to-volume ratio increases. These effects influence how the transport of mass, momentum and energy through the channel is modeled [55].To account for rarefaction, the main micro-effect that results from the shrinking of flow channels, previous studies that model the mechanics of gaseous flows through micro devices, have used the classical continuum approach and incorporated slip boundary conditions, thermal creep, viscous dissipation, and compressibility effects into the momentum balance [55]. However for very small systems, it may be advantageous to model fluid flows as a collection of molecules rather than as a continuum of matter [55]. This is because the continuum approach requires the molecules to be in thermodynamic equilibrium [69].

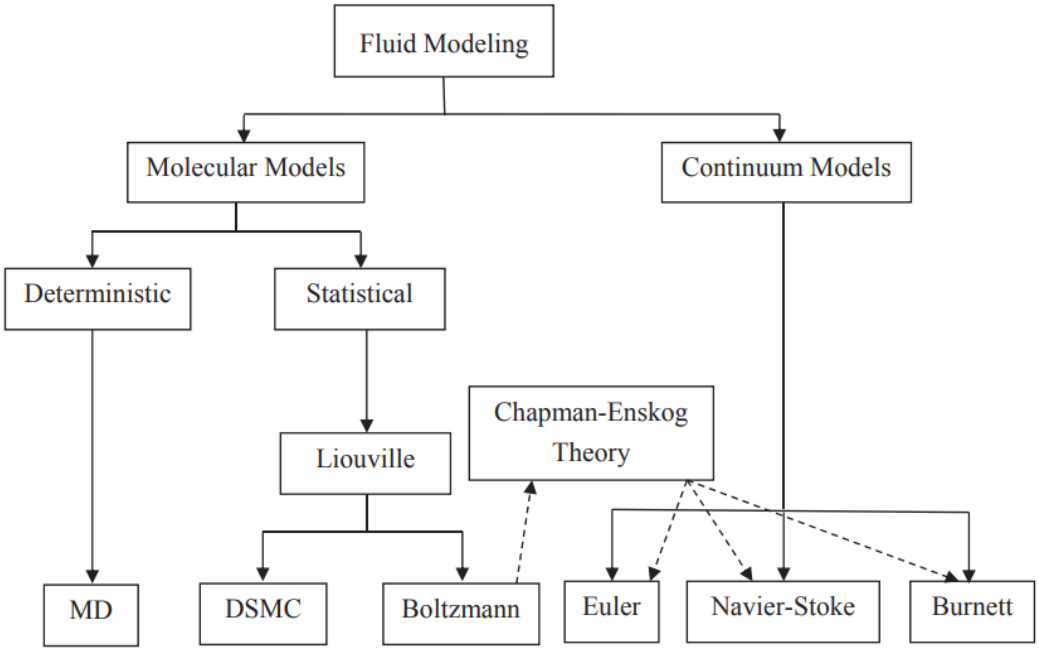

Figure 11: Fluid flow modelling approaches (from [70])

2.6.3 The Knudsen Number

Fluid flows can be modelled in various flow regimes, depending upon the mean free path, or average distance traveled by a molecule, and the characteristic dimension of the flow channel. When fluid flows begin to deviate from the continuum flow regime, they can be characterized using different molecular transport models. The Knudsen number is the most fundamental parameter that is used to determine the degree of rarefaction and to differentiate between various flow regimes. The Knudsen number is the ratio of the mean free path,□□, to the characteristic length, L of the flow channel

$$Kn = \frac{\lambda}{L} \tag{17}$$

The mean free path is the distance a molecule travels between collisions. The characteristic dimension is generally defined as the hydraulic diameter or the depth of the

channel [68]. In complex geometries, the characteristic length is defined from local gradients (e.g., □□□□□) which results in a "local rarefaction number" [69]. For example, using the density, □, the characteristic length can be defined as

$$L = \frac{\rho}{\left|\frac{\partial \rho}{\partial y}\right|} \tag{18}$$

The Knudsen number characterizes the significance of rarefaction effects, which become increasingly important as the characteristic length of the channel approaches the mean free path of the molecules. For small Knudsen numbers, collisions between molecules dominate the flow and interactions; as the size of the system is reduced and the Knudsen number increases, collisions between the molecules and boundary wall surfaces are increasingly more important and molecular dynamics must be considered. Thus, the Knudsen number is a measure of the validity of the continuum model [55].

Rarefaction is a conceptual term that is used to describe a transition from continuum flow regime models to molecular transport models. Once flows cannot be described using the continuum model, local properties, like density, can no longer "be defined as averages over elements large compared with the microscopic structure of the fluid" [55]. The inherent nature of the molecules becomes increasingly important as the flow channel begins to interfere with the movement of the molecules. Finally, it is important to note that the mean free path is a conceptual quantity that is defined for hard sphere molecules, which is reasonable for continuum methods but may not apply in other flow regimes [71].

The Knudsen Number differentiates the following flow regimes:

1. For Kn < 10^{-3}, the flow is in the continuum flow regime and is accurately modeled by the Navier-Stokes equations with classical no-slip boundary conditions [56]
2. For 10^{-3} < Kn <10^{-1}, the flow is in the slip flow regime and the Navier-Stokes equations are adequately applicable, provide that boundary conditions like velocity slip and a temperature jump are taken into account at the walls to account for rarefaction effects that first become significant at the wall [56]
3. For 10^{-1} < Kn <10, the flow is in the transition flow regime and the Navier-Stokes equations are no longer valid here. The intramolecular collisions are not negligible and should be taken into account [56]
4. For Kn>10, the flow is in the free molecular flow regime and the occurrence of intermolecular collisions is negligible compared with collisions between the gas molecules and the walls [56]

In classical fluid mechanics that is focused on macroscopic flow, the impact of the Knudsen layer on the overall flow is largely negligible. For leaks that occur through the mated screw connections of NG fittings, much of the literature has assumed that these flows will occur in the continuum viscous region, where the channel dimension is much greater than the molecular mean free path of the molecules and the flow is dominated by intermolecular collisions (collisions between molecules). It may be that in reality, gaseous fuel leakage will occur through channels that are similar in size to the molecular mean free path of the molecule. If this is the case, then intramolecular collisions, collisions between the molecules and the walls, must be accounted for when estimating and quantifying gaseous fuel leakage.

Finally, the Knudsen Layer (KL) is the boundary layer that forms over a solid surface as a gas flows. It is in the order of the mean free path of the molecule. See Figure 12 for a diagram of the boundary layer. For gases which flow very close through a solid surface, conventional fluid dynamic models may not be appropriate because the assumptions of quasi thermodynamic-equilibrium and the associated no-slip boundary condition are no longer accurate [72]. Gases that flow near the surface exhibit the finite velocity and non-Newtonian stress/strain-relationship. For a gas molecule to leak, it must separate itself from the bulk gas and contact the leak hole within the boundary formed by the solid surface. This mode for molecular transport is best characterized with statistical analyses.

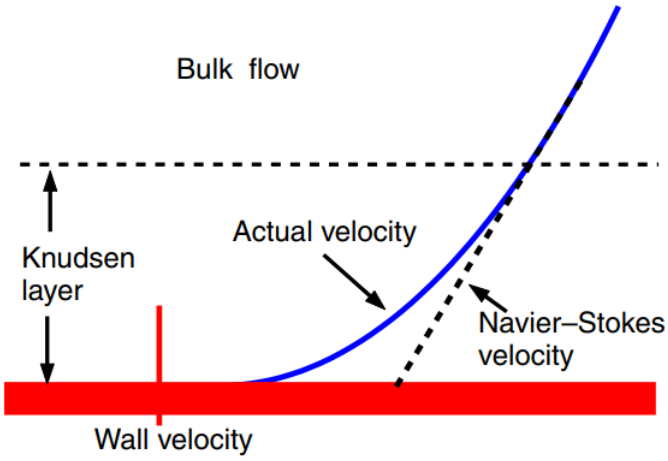

Figure 12: Knudsen layer formed at the boundary (from [73])

2.7 Summary of Findings from the Literature Review

In the previous sections, an overview of the literature related to gaseous fuel leakage is presented. Most of the literature associated with gaseous fuel leakage from low-pressure NG infrastructure assumes that gaseous fuel leaks through passages created by defects amongst the mated screws defects can be modelled as smooth microchannels with constant

height in the continuum flow regime. As a result of these assumptions, the expectation is that H_2 should leak much faster than other molecules that are larger, such as CH_4. However, these assumptions may not apply for leaks in NG infrastructure since the leakage path may be tortuous and with significant wall interactions. Additionally, there is limited experimental research to show that the traditional fluid mechanics theories in the continuum flow regime can accurately characterize leakage from NG infrastructure. To contribute to the understanding of the governing flow regime for gaseous fuel leaks, this thesis will experimentally evaluate the mechanism of gaseous fuel leakage using NG infrastructure simulated leak rigs.

Lastly, a review of the literature resulted in the discovery of results which suggest that H_2 and NG may leak at the same rate in [36], one of the few papers that experimentally assesses gaseous fuel leakage from NG infrastructure. The authors' explanation for the same rates of leakage in some of their experiments is the possibility of entrance effects governing this flow [36]. In this thesis, the possibility that entrance effects could explain the observed discrepancy in the literature is assessed experimentally.

3 Goal and Objectives

The goal of this study is to evaluate the impacts of H_2 on gaseous fuel leakage from low-pressure NG infrastructure and to develop an understanding of the mechanism of gaseous fuel leakage from NG piping systems. The objectives established to accomplish this goal are listed below:

1. Complete a thorough literature review of gaseous fuel leakage from NG infrastructure.
2. Evaluate gaseous fuel leakage from an existing NG system for H_2 and blends of H_2 with NG.
3. Collaborate with SoCalGas to compare and verify findings from Task 2.
4. Apply and evaluate a mitigation measure to stop leaks for blends of H_2 with NG.
5. Construct an experimental leakage rig to simulate gaseous fuel leakage.
6. Develop a potential theory of the mechanism of gaseous fuel leakage in low-pressure NG infrastructure.

In this work, existing low-pressure NG piping infrastructure is used as a platform to evaluate the leakage from NG infrastructure on the customer-side of the meter for blends of pure NG, a 90% NG and 10% H_2 by volume mixture, and pure H_2. In addition, results from similar experiments conducted by the Southern California Gas Company for a simulated leak environment are presented and used to validate independent experimental findings. Further, a potential leak mitigation strategy is evaluated to determine if it is capable of eliminating gaseous fuel leakage from an identified faulty piping system. Finally, a theory is proposed that explains the leakage rates observed in previous studies and in the current

study. This theory may more accurately characterize typical gaseous fuel leakage from National Pipe Thread (NPT) fittings in low pressure gas infrastructure.

4 Methodology

To further investigate gaseous fuel leakage, various experiments were conducted at the National Fuel Cell Research Center (NFCRC). First, a series of leakage tests were conducted in two isolated sections of existing NG infrastructure in the laboratory facilities of the NFCRC. Second, an experimental leakage rig was constructed using needle probes to study the entrance effects on gaseous fuel leakage. Third, experiments were conducted at Southern California Gas Company facilities using an experimental rig for leak simulation and measurement. Finally, after the finding that gases were leaking from existing NG infrastructure, a mitigation strategy was assessed to determine whether and how well it could reduce gaseous fuel leakage.

4.1 Experimental Study of NG Leakage using Commercial Building Infrastructure

Two sections of existing NG pipeline infrastructure were developed for testing procedures to study emissions from infrastructure and impacts of various mixtures of H_2 and NG blends including pipeline parts, compressor parts, meter set, and customer appliances. The existing infrastructure evaluated in this study was constructed in 1987 and is comprised of typical National Pipe Thread commercial stainless-steel pipes with fittings, valves, and support clamps as installed within a cement tilt-up construction building used for laboratory experiments.

Chosen sections of NG infrastructure have previously been used in research involving energy conversion and combustion activities and is part of the low-pressure piping network in the building. Typical pressures for the sections are approximately 2.5 kPa, approximating the pressures of residential NG piping. Pipe sections were isolated via valves and, apart from additional fittings and transducers, the piping networks were left

without further modifications from their initial state. The two sections of piping are separate from each other and each has unique pipe properties. Table 2 presents the volume, pipe length, pipe diameter, and number of joints of each piping system studied in this analysis. A picture of piping section A is show in in Figure 13.

Table 2: Piping section characteristics

Piping Section	Volume (m^3)	Pipe Length (m)	Pipe Diameter	# of Joints
A	0.0261	14.0	1 ½ NPT	24
B	0.013	7.01	1 ½ NPT	14

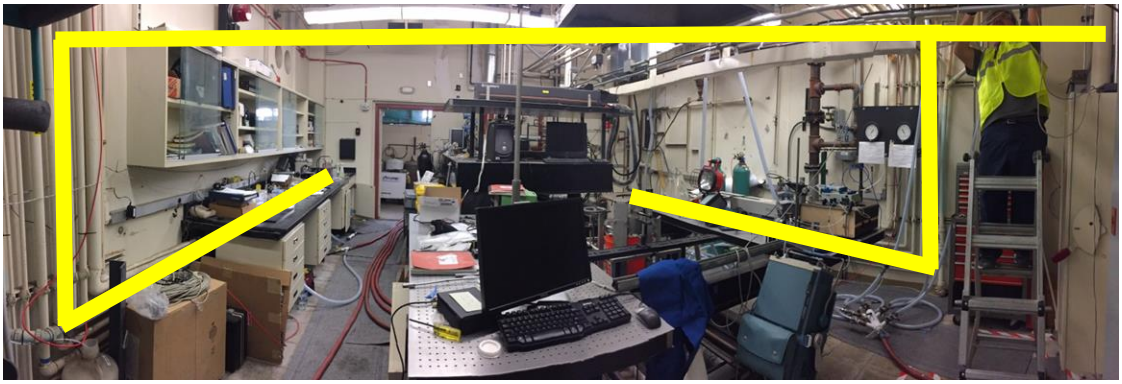

Figure 13: Test cell where the tests were conducted for piping section A (NG infrastructure is highlighted in yellow)

The test sections were inspected for leaks with handheld combustible gas sensors with reported sensitivities down to 100 ppm of methane. Figure 14 illustrates sites identified with significant gas leakage. In addition to the sensors, liquid leak detection solutions were used to identify sites of NG leaks. The leak areas identified occurred at the

joints, valves, or connections between pipe fittings. It is also worthwhile to note that no mercaptans were sensed via olfactory during this study.

Figure 14: Images of various detected NG leaks within the test infrastructure

To evaluate and quantify the impacts on emissions from commercial building infrastructure from fuel blending of H_2 into the NG supply, pure NG, pure H_2 gas, and a blend composed of 10% H_2 and 90% natural (by volume) gas were individually tested in the test sections. Blends were injected at initial pressures of 46 inH_2O (1.6 psig) and allowed to naturally leak from the two separate existing NG infrastructure test sections. Test sections were isolated from any additional gas supply sources and all outlet or inlet valves were closed. To ensure accurate blends of the gas, the piping system was flushed with the desired dilution gas before every injection. The dilution gas (either pure H_2 or pure NG) was injected at a pressure of 12 psig (2.98kPa) and vented after one minute. This

process was repeated multiple times before the injection of the desired gas. For the case of pure H_2 or pure NG, after several flushing events, the pure gas was injected to produce an initial pressure of 46 inH_2O (11.4 kPa) to start each experiment. In the case of the 10% H_2 and 90% NG blend, the piping was first flushed with NG several times. This was followed by H_2 injection to 46 inH_2O (11.4 kPa) to achieve a mixture of 10% H_2 in NG.

To characterize the variation in leakage between tests, the pressure in the piping system was measured and recorded on a per minute basis for each leak test. A Setra 209 pressure transducer and a DENT data logger were used to record and log the pressures. Additionally, an Omega MP2 Type T thermocouple was used to record temperature vs time.

4.2 Experimental Leak Rig

An experimental leak rig was constructed and used by the Southern California Gas Company (SoCalGas) to evaluate impacts on gas leakage associated with H_2 blending with NG. SoCalGas assessed blends of 100% NG and blends with 6-8% H_2 in NG (by volume). Each gas blend was tested at two initial pressures – 417 kPa and 3.0 kPa. Figure 15 shows the SoCalGas experimental test rig consisting of regulators, a laminar flow element, a pressure transducer, a thermocouple, valves, fittings, and stainless steel piping and fittings. Before each leak test the rig was tested with a liquid leak detector and portable gas detectors to assure that it was gas-tight. A gas chromatograph was used to measure gas composition before and after the test runs. To meet the minimum pressure for the gas chromatograph (GC), a syringe was used to extract the sample and inject it onto the GC. Testing procedures consisted of creating a fixed simulated leak with a needle valve or using a brass end cap that was loosened to produce a specific leak circumstance. A pressure

transducer recorded the pressure every minute throughout the entirety of tests, with the length of a single test at approximately 7 hours.

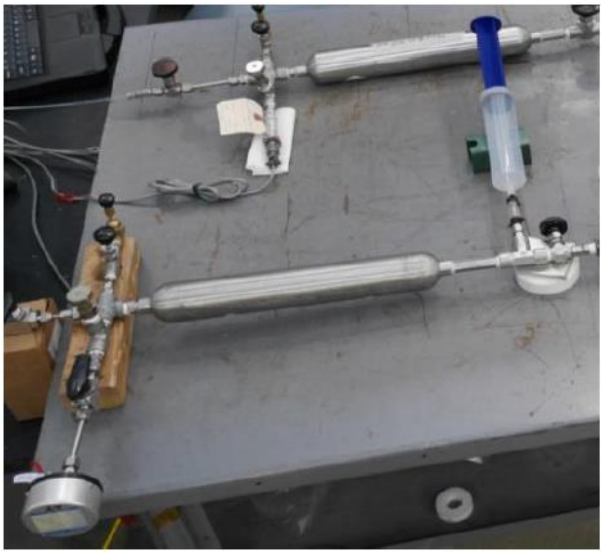

Figure 15: SoCalGas H_2 leak study experimental setup

4.3 Mitigation Strategy Assessment

One of the two sections of existing NG piping that was leaking (Section B described in Table 2) was isolated to assess a potential leak mitigation measure. Prior to deploying the mitigation measure, the piping was found to contain significant leaks for all gas blends. After characterizing the pipe leakage with gas injection and leakage tests, a local piping restoration company, Pipe Restoration Inc, offered to restore this section of the NG piping infrastructure. This company specializes in coating the inner walls of piping with a copper-based-epoxy (see Figure 16). The pipe is first prepared for the internal coating through preheated, air drying, and a sandblasting pretreatment. The final stage of the ePIPE ® restoration involves a pressurized flow of a slug of the copper epoxy that leaves a thin

coating behind, lining the pipe. Additionally, as part of the restoration procedure, some threaded caps and valves were replaced to ensure minimal leakage. Once the epoxy cured, the piping section was retested with the original gas blends at the same pressures via the procedure for leak testing described in 4.1.

Figure 16: Pipe fitting coated with the copper epoxy

4.4 Entrance Length Test Rig

An experimental leakage rig was built to explore the effects of entrance length and exit length on gaseous fuel leakage from low-pressure piping systems. This test rig was built using blunt needle probes of various diameters and lengths to study the impact of entrance effects on leakage of H_2 and NG. This test rig was constructed primarily because authors of the seminal paper on H_2 leakage [36] attribute the similar leak rates observed for H_2, CH_4, and C_3H_8 to entrance effects. A series of tests were performed to test entrance length and underdeveloped flows of H_2 and NG.

The experimental leakage test rig (Figure 19) was pressurized with the desired gas of interest (either H_2 or NG). The flowrate of each of the gases was measured with a bubble

meter for a range of pressures. Blunt needle probes of various diameters and lengths were used to vary entrance length (See Figure 17). These blunt needle probes were purchased from Grainger (item number 5FVA7). They have an internal diameter of 0.016 in (0.4064 mm) and total length of 2.125 in (53.975 mm). To vary the entrance length, the length was modified and reduced to 0.125 in (3.175 mm) for some of the tests. The flow rate of H_2 and NG was tested at different pressures for each of the blunt needle probes with varied lengths. Finally, in these experiments, the relationships between pressure, flow rate, rate of pressure drop, and Reynolds number were evaluated to analyze the leakage. The flow rate was measured using bubble flowmeters of various sizes while the upstream of probe pressures were set to a range up to 1.45 psi (10 kPa).

Additionally, the test procedures were repeated for a simulated leak using a precision needle valve equipped with a scale on the handle that allowed for precision control of the flow (See

Figure 18). The precision needle valve was purchased from Swagelok and the part number is SS-SS4-VH. When the valve is fully open it has a flow coefficient of 0.004. The orifice diameter of this valve is 0.81mm. Flowrates were measured for various different valve openings.

Figure 17: Blunt probe needle used for testing the effects of entrance length

Figure 18: Needle valve with a Vernier handle that was used for experiments

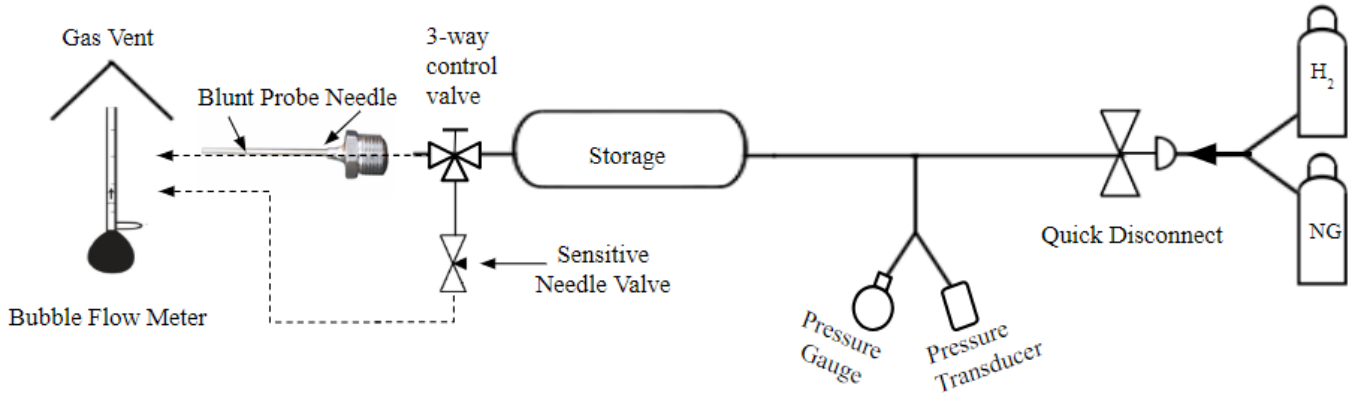

Figure 19: Experimental setup of the leakage rig

4.5 Packed Capillary Tube Test

An experimental leakage rig similar to the one shown in Figure 19 was built to explore the effects of a tortuous path on gaseous flows of H_2 and NG. Instead of using the blunt

needle probes, a packed capillary tube column was used. The packed capillary tube is made of stainless steel and Pyrex glass packing material and it was intended to be used for gas chromatography. It has a total length of 5 ft (1.5 m) and an inner diameter of 0.0827 in (2.1 mm). The packed capillary tube was purchased from Sigma Aldrich and the item number is 13044-U. Similar to the entrance length leakage tests in the previous section, the flowrate was measured with a bubble flow meter for a range of pressures up to 10 psi (69 kPa). The system was vented and flushed multiple times with the desired gas to ensure an accurate blend of each gas in each experiment. Finally, the leakage ratio, flowrates, and pressures were evaluated to compare the flow through the tortuous path that was created by the packing material in the column.

5 Results

5.1 Investigating Leakage in Existing NG Infrastructure Section A

An analysis of the pressure vs time dynamics for each gas blend as injected into one of the existing low-pressure NG test sections is presented in Figure 6 to observe the relative leakage rates for each gas mixture in the same existing, isolated NG piping system. Figure 20 shows the average instantaneous pressure of each gas blend that was measured every 15 minutes in piping section A over a period of 7 days. The error bars correspond to one standard deviation of three separate data sets that were taken for each of the gas blends. Table 3 summarizes the results from the leakage tests in existing NG infrastructure.

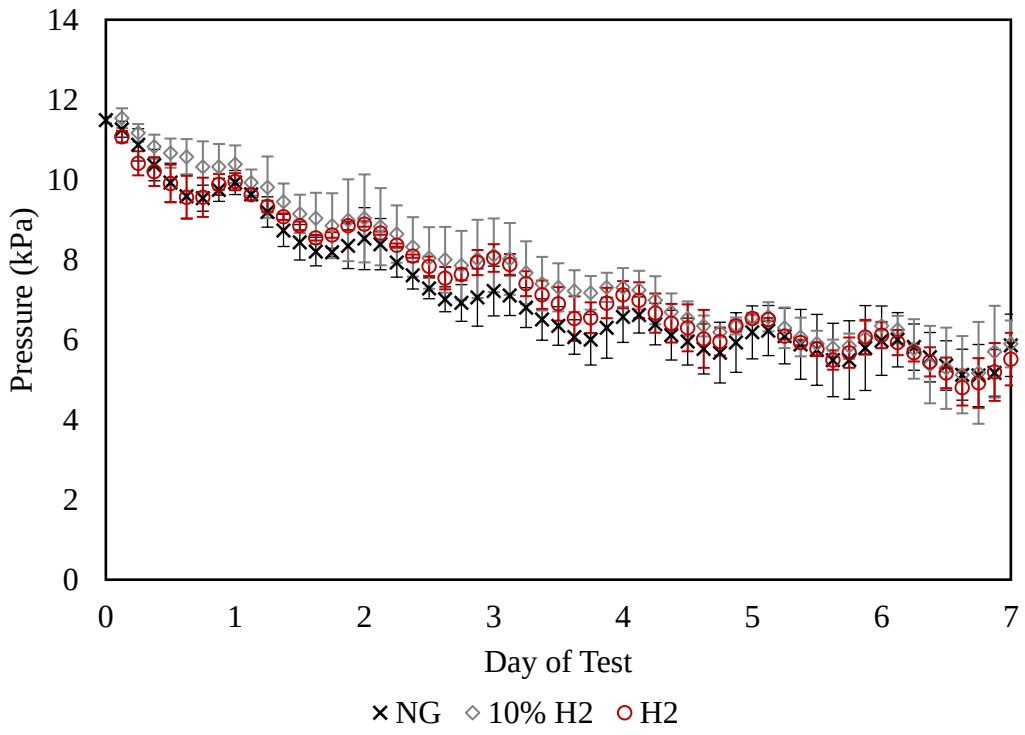

Figure 20: Change in pressure vs time of various gas mixtures in piping section A

Table 3: Summary of leak tests in piping section A

Gas	H_2	10% H_2 with NG	NG
Average Pressure Drop Rate (kPa/hr)	0.99	0.95	1.04
Maximum Standard Deviation Observed (kPa)	0.83	1.36	1.46

The pressure oscillations observed in Figure 20 are due to diurnal temperature changes. The temperature measurement verified ideal gas behavior and are consistent with similar pressure oscillations due to temperature changes that were observed by Ge and Sutton in [59]. Within experimental error and deviations (as indicated by the error bars), all gas blends are shown in Figure 20 to leak at the same rate. The pressure profiles of each of the gases overlap and are within the range of experimental errors measured.

All the gas blends seemed to reach around 5.72 - 5.97 kPa (23-24 inH_2O) after 7 days of testing. For all gaseous fuel blends, it was observed that half of the gas injected into the piping system leaked within 7 days. These results suggest that the gas composition (H_2 or NG) may not be a significant factor in determining the leakage rate of a gaseous fuel from existing low-pressure NG piping systems.

5.2 Experimental Leak Rig Results

Gas leakage for blends of 100% NG and 5% (vol) of H_2 with 90% (vol) NG were evaluated using the simulated leak environment at SoCalGas facilities (described above) using a needle valve to control the leakage rate. These results are shown in

Figure 21. The leakage was evaluated at two different initial pressures starting at 3.20 kPa and 417 kPa. A similar observation can be made for both the high pressure and low-pressure tests: NG and H_2-NG blends appear to leak at the same rate. No significant

difference was observed in the pressure drop characteristics between the NG and blended gas tests. In addition, the average H_2 content (measured by the GC) in the gas remaining in the rig after the leakage tests was within 1% of the original mixture content (see Table 4). This suggests that if a blend of 5% H_2 with NG is injected into a system with some gas leakage, H_2 will not preferentially leak out of the system.

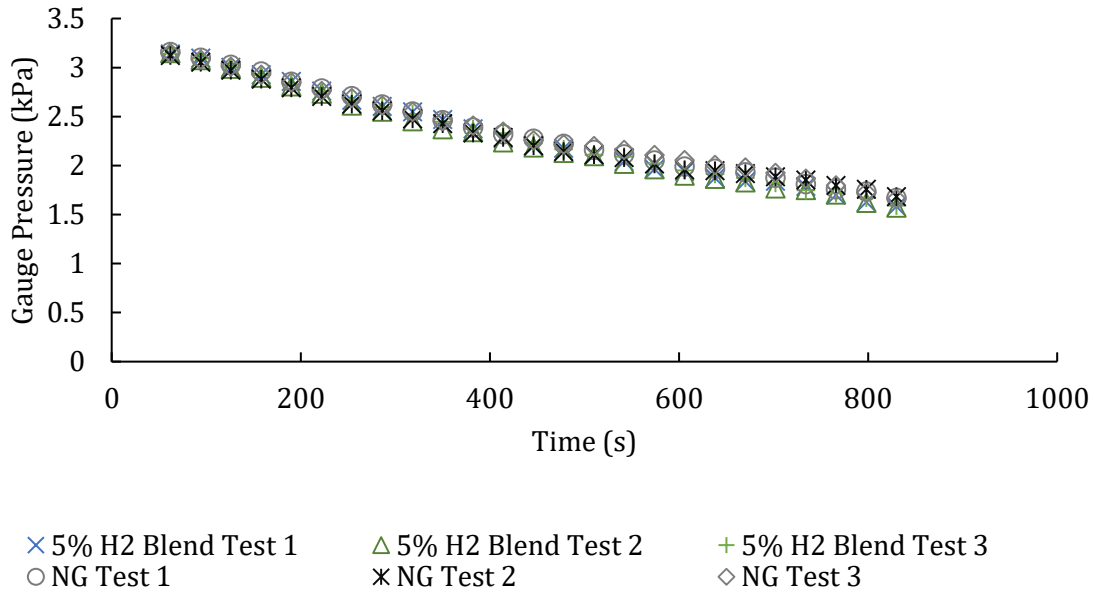

(a) Results for test with initial pressure of 3.20 kPa

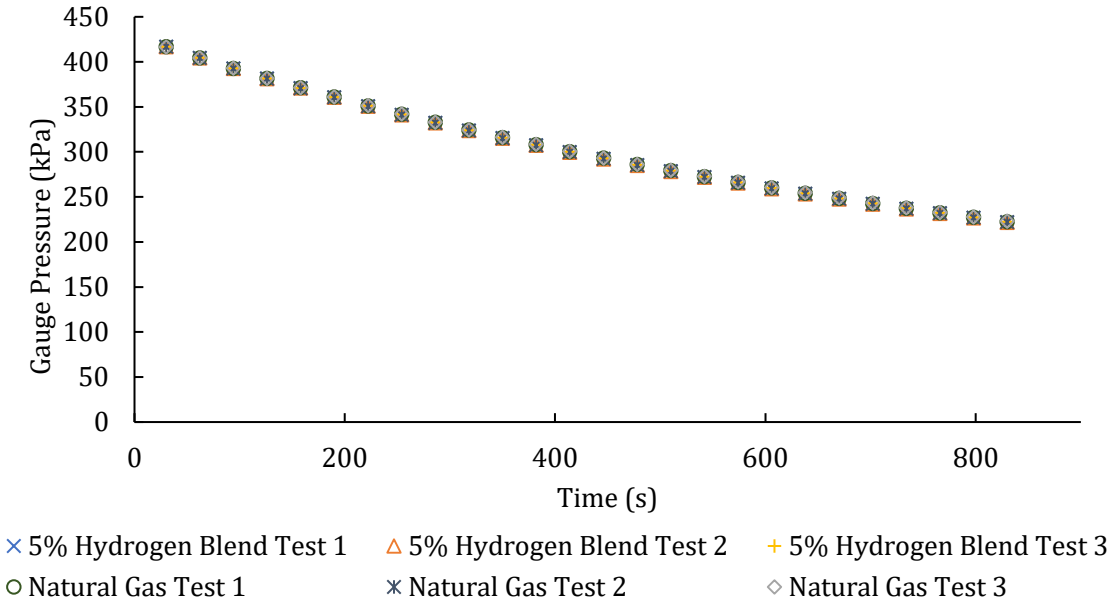

(b) Results for test with initial pressure of 417 kPa

Figure 21: Change in pressure vs time for pure NG blend and 5 vol% H_2 with NG at initial pressures of (a) 3.20 kPa and (b) 417 kPa

Table 4: Summary of average H_2 content % change

Starting Pressure	*Gas*	*Average H_2 Content %Change*
60 psig	Pure NG	N/A
	5% H_2 with NG	-0.591%
12 inH_2O	Pure NG	N/A
	5% H_2 with NG	-0.577%

5.3 Evaluation of a Leak Mitigation Strategy in Piping Section B

To assess the effectiveness of one leak mitigation strategy, piping section B (see Table 2) for characteristics) of existing NG infrastructure was selected for ePIPE® application (as describe above). Piping section B was observed to have much higher rates of leakage than piping section A. A summary of the results is provided below in Table 5.

Table 5: Pressure drop in piping section A and B

Average Pressure Drop Rate	H_2	10% H_2 with NG	NG
Piping Section A (kPa/hr)	-0.04	-0.03	-0.04
Piping Section B (kPa/hr)	-0.16	-0.18	-0.16

The average pressure drop rate of piping section B was approximately twice as much as the average pressure drop rate of piping section A for each gas blend test. Thus, it was decided that the mitigation measure would best be evaluated in piping section B, the piping with higher leakage. Since the leakage in Section B was so significant each test of the piping in its original state lasted two days.

Like the gaseous fuel leakage behavior observed in piping section A, there was no notable difference in the leakage rates between different gas mixtures in piping section B.

The average pressure drop rate for the pure H_2 blend was the same as the average pressure drop rate for the pure NG blend and the H_2/NG blend within experimental error. Though, the 10% H_2 blend appeared to have a slightly higher pressure drop rate than the other blends, the leakage difference falls within the pressure transducer accuracy bounds (0.25% FS of 0-2 psig) and therefore this difference is not statistically significant. Thus, the initial findings for this set of NG piping are similar to the findings of the leakage tests in piping section A – gas mixtures of H_2 and NG can leak at approximately equivalent rates from the existing low-pressure NG piping systems.

After characterizing the leakage in piping section B, ePIPE® was applied and the piping was retested with the same blends and significantly pressure drop rates were observed. Figure 22 compares the pressure of piping in its original state and after it was repaired.

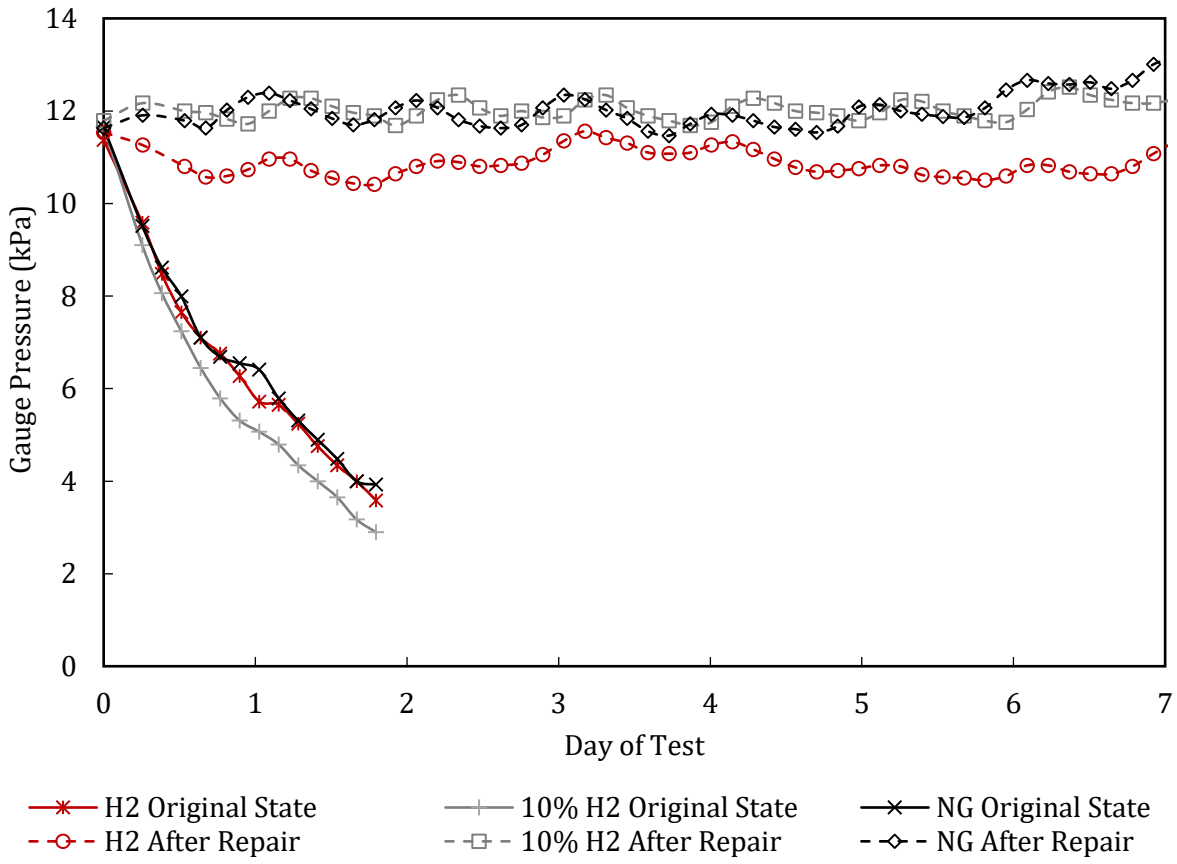

Figure 22: Comparison of change in pressure vs time of NG and H_2 for piping section B in its original state and after repair

After piping section B was repaired, it was re-inspected for leaks with a liquid leak detecting solution and handheld combustible gas leak detectors. No leaks were detected using these techniques. It is likely that the epoxy filled in most of the cracks and defects in the piping, reducing the distance between the imperfectly mated screws and therefore eliminating the gaseous fuel leakage. No leakage was experimentally observed after the mitigation measure was applied for a period of seven days. Thus, it is concluded that the application of the copper epoxy mitigation approach was successfully able to contain all gas blends.

5.4 Entrance Length Experimental Results

The purpose of this study was to research whether the effects of entrance length can give insight as to why NG and H2 leak at the same rate through typical leaks in threaded fittings of low-pressure NG infrastructure. The results of the experiments with a needle probe with a length to diameter ratio (L/D) of 7.81 are presented in Figure 23, while those for a needle probe with a L/D ratio of 133 are plotted in Figure 24. Selected data points from Figure 23 and Figure 24 are presented in Table 6 along with a calculated leakage ratio. The leakage ratio is a quantity that represents the leak rate of H_2 divided by the leak rate of NG. This value represents how much faster H_2 leaked in comparison to NG for each of the measurement conditions.

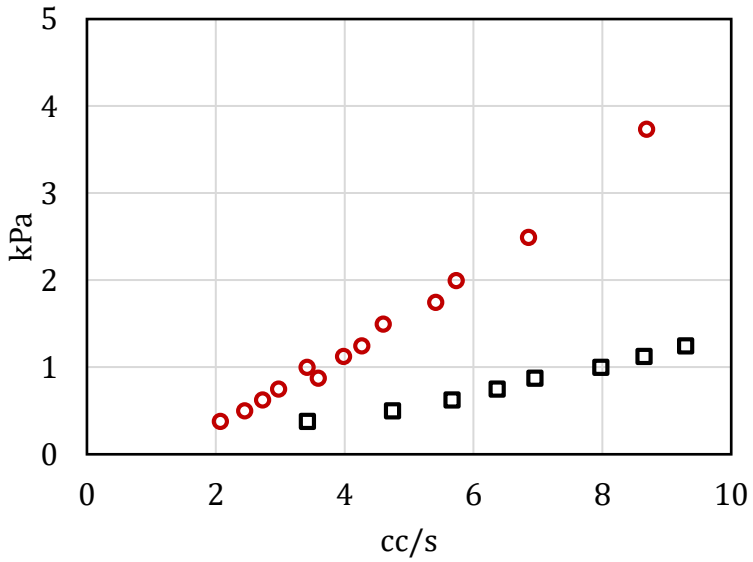

Figure 23: Pressure vs flow rate for H_2 (□) and NG (○) through a needle prob with L/D= 7.81

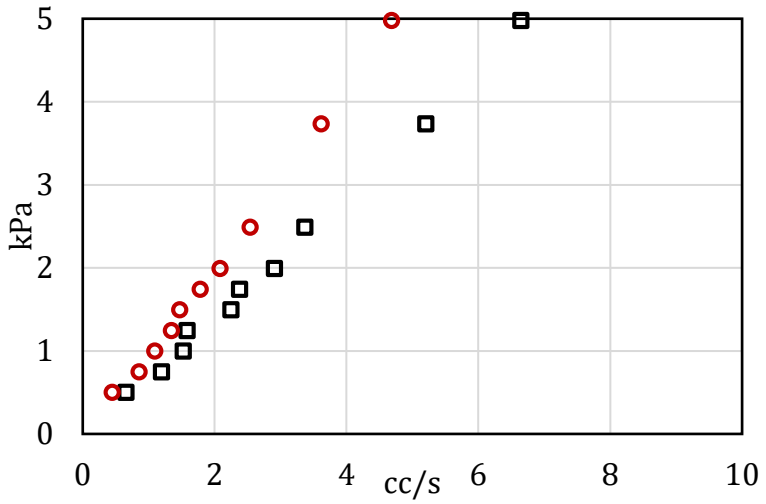

Figure 24: Pressure vs flow rate for H_2 (□) and NG (○) through a needle prob with L/D= 133

For the tests with the L/D ratio 7.81, the probe length was much smaller than the entrance length required for fully developed flow for nearly all of the flow rates tested. The total length of this probe is 3.175 mm and the calculated entrance lengths for fully developed laminar flow is shown in Table 7. For this needle probe, the leakage ratio of H_2 to NG is between 1.94 and 2.33. For fully-developed flows in the laminar regime, the leakage ratio should be 1.29. The values estimated from the leakage ratio suggest that the flows are all experiencing non-fully developed conditions so that the theory for laminar flow described above does not apply. When these entrance length effects dominate and leakage is controlled by a regime that is not fully developed, it appears that H_2 leaks 2-3 times faster than NG. This suggests that entrance effects may result in higher H_2 leak rates than predicted by laminar flow theory.

For the case with L/D=133, the total length of the needle probe was 53.975 mm, which is much longer than the entrance length required for fully developed laminar flow

for most of the flowrates tested. For this simulated leak it is known that the majority of the flow is fully-developed laminar flow (see data presented in Table 8). In addition, the laminar flow regime behavior of H_2 leakage can be verified by observing the linear relationship between pressure and flow rate in Figure 24. Thus, in this laminar flow regime with L/D = 133 the ratio of H_2 leakage rate to NG leakage rate is measured between 1.33 and 1.53, which is consistently higher than, but close to the fully developed laminar flow theory of 1.29. This suggests that entrance length regime leaks would produce higher than fully-developed laminar flow H_2 and NG leakage rates, which may be due to either turbulence or diffusion-controlled flow conditions at the entrance. The explanation of Swain and Swain [36] that the similar leak rates of H_2, CH_4, and C_3H_8 they observed in realistic leak scenarios may be due to entrance effects is hereby questioned.

Results from both of the needle probe experiments suggest that leakage that is controlled by entrance effects produces higher H_2 leak rates than laminar flow theory suggests. A major finding from these experiments with the needle probes is that entrance length effects do not explain the similar gaseous fuel leakage rates for H_2 and NG through threaded NG fittings observed by Swain and Swain [36] and in the current work. Thus these results suggest that entrance effects do not explain the similar leak rates of H_2 and NG.

Table 6: Selected data points from Figure 23 and Figure 24 and calculated leakage ratio

Pressure (kPa)	Flow Rates (cc/s)				Leakage Ratio H_2/NG	
	L/D =133		L/D =7.812			
	H_2	NG	H_2	NG	L/D =133	L/D =7.812
0.50	0.66	0.45	4.74	2.45	1.47	1.94
0.75	1.19	0.85	6.37	2.97	1.40	2.14
1.00	1.53	1.09	7.98	3.42	1.40	2.33
1.49	2.25	1.47	10.3	4.60	1.53	2.25
1.74	2.38	1.78	11.5	5.42	1.33	2.13
1.99	2.91	2.08	12.7	5.73	1.40	2.21
2.49	3.37	2.54	15.4	6.86	1.33	2.24
3.73	5.20	3.62	20.0	8.69	1.44	2.30
4.98	6.65	4.69	24.1	10.8	1.42	2.24

Table 7: Reynolds number for H_2 and NG at various pressures through a probe needle with L/D= 7.812

Pressure (kPa)	Reynolds Number		Entrance Length (mm) if laminar	
	H_2	NG	H_2	NG
0.37	106	393	2.5	9.2
0.62	175	518	4.1	12.1
1.00	246	650	5.8	15.2
1.49	319	873	7.5	20.4
1.99	391	1089	9.1	25.5
2.49	475	1303	11.1	30.4
3.73	617	1651	14.4	38.6
4.98	746	2047	17.4	47.8

Table 8: Reynolds number for H_2 and NG at various pressures through a probe needle with L/D= 133

Pressure (kPa)	Reynolds Number		Entrance Length (mm) if laminar	
	H_2	NG	H_2	NG
0.50	20	85	0.4	1.6
0.75	37	161	0.8	3.1
1.00	47	207	1.0	4.0
1.49	69	279	1.5	5.4
1.99	90	395	2.0	7.6
2.49	104	483	2.3	9.3
3.73	161	687	3.5	13.2
4.98	205	890	4.5	17.1

5.5 Precision Needle Valve Tests Results

In this set of experiments, a needle valve with a Vernier handle was used to simulate a controlled leak. The valve was carefully opened to two different revolutions and the flowrates of H_2 and NG were measured with bubble meters.

5.5.1 Needle Valve Test Results for 1 revolution

In the first case, the valve was opened by one revolution. This was carefully configured using the Vernier handle. The gauge pressure and flowrates measured for this case are shown in Figure 25 pressures between 7 and 69 kPa for pure blends of H_2 and NG. Additionally, the leakage ratio is calculated below in Table 9. For these flows, the upstream and downstream pressure ratios are below the required conditions for sonic, or choked flow.

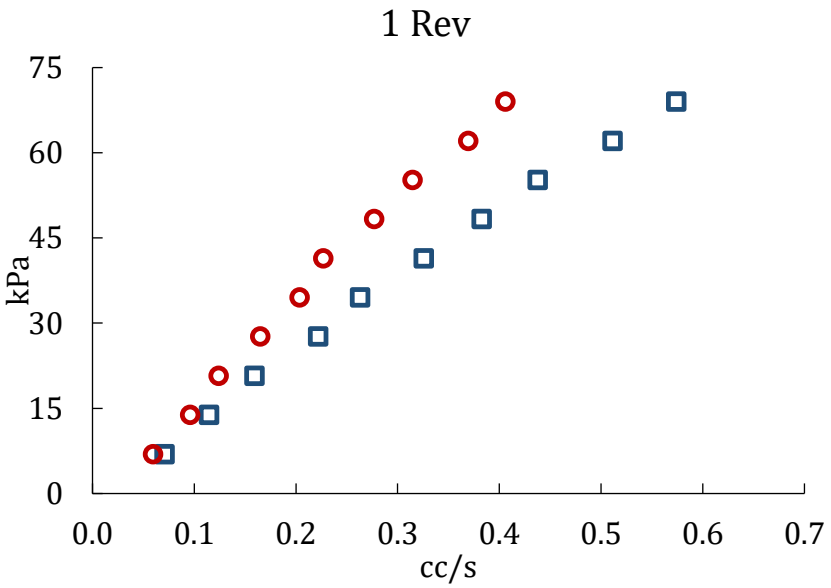

Figure 25: Pressure vs flow rate for H_2 (□) and NG (○) through a needle valve that was opened one full revolution.

The results for this test are similar to the results for the previous experiment with a probe needle. As the pressure increases, the difference in leakage between H_2 and NG also increases. For this case the leakage ratio ranges from 1.19 to 1.44. At the two lowest pressures measured, 6.92 and 13.8 kPa, the leakage ratio is 1.19 and the pressure of 41.4 kPa corresponds to the leakage ratio of 1.44. This data seems to suggest that leakage ratio increases with pressure, although the correlation is not as strong as in the case with the probe needles.

Table 9: Pressure, flow rates and leakage ratio for H_2 and NG flows through a needle valve that is opened one full revolution

1 Rev			Leakage Ratio H_2/NG
Pressure (kPa)	Flow Rates (cc/s)		
	H_2	NG	
6.92	0.071	0.060	1.19
13.8	0.115	0.096	1.19
20.7	0.159	0.124	1.28
27.6	0.222	0.165	1.35
34.5	0.263	0.204	1.29
41.4	0.326	0.227	1.44
48.3	0.383	0.277	1.38
55.2	0.438	0.315	1.39
62.1	0.511	0.370	1.38
69.0	0.574	0.406	1.41

Additionally, the entrance length and Reynolds number have been calculated for these flows and are shown in Table 10. The calculated Reynolds numbers, based upon experimental data, suggest that both the H_2 and NG flows should be in the laminar regime for the entirety of the pressure range tested. However, the calculated entrance length suggests that the entrance length required for fully developed flow is much larger for NG than for H_2.

Table 10: Calculated entrance length and Reynolds number for a needle valve that is opened one full revolution

Pressure (kPa)	Reynolds Number		Entrance Length (mm)	
	H_2	NG	H_2	NG
6.92	1.03	4.67	0.048	0.217
13.8	1.67	7.51	0.078	0.350
20.7	2.32	9.73	0.108	0.453
27.6	3.23	12.9	0.150	0.601
34.5	3.83	15.9	0.178	0.742
41.4	4.74	17.8	0.221	0.827
48.3	5.57	21.7	0.260	1.01
55.2	6.37	24.6	0.297	1.15
62.1	7.44	28.9	0.347	1.35
69.0	8.36	31.8	0.389	1.48

5.5.2 Needle Valve Test Results for two revolutions

In this section, the results for the test with a needle valve that is open to two revolutions are presented. The flowrates were measured for a pressure range between 6.89 and 68.95 kPa for both H_2 and NG blends. These results are show below in Figure 26 and Table 11.

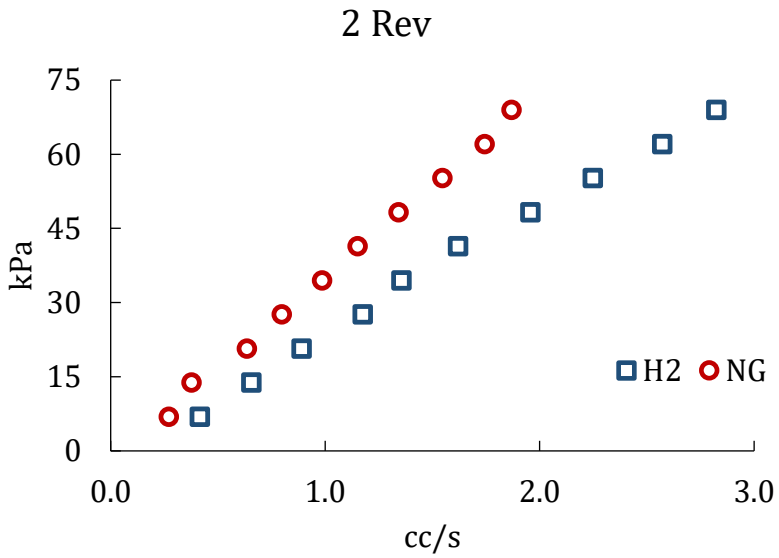

Figure 26: Pressure vs flow rate for H_2 (□) and NG (○) through a needle valve that was opened to two revolutions

Unlike the previous tests, the results do not seem to suggest that the leakage ratio is increasing with pressure. It may be that flow through the needle valve behaves more like flow through an orifice rather than flow through a cylindrical duct. The leakage ratio is 1.54 for the lowest pressure measured, 6.89 kPa, and 1.51 for the high pressure measured, 68.95 kPa.

Table 11: Pressure, flow rates and leakage ratio for H_2 and NG flows through a needle valve that is opened two full revolutions

2 Rev			Leakage Ratio
	Flow Rates (cc/s)		
Pressure	H_2	NG	H_2/NG
6.89	0.417	0.271	1.54
13.79	0.657	0.376	1.74
20.68	0.890	0.636	1.40
27.58	1.175	0.798	1.47
34.47	1.357	0.986	1.38
41.37	1.620	1.151	1.41
48.26	1.958	1.342	1.46
55.16	2.248	1.547	1.45
62.05	2.572	1.744	1.48
68.95	2.824	1.869	1.51

The Reynolds number and entrance length were also calculated for this experiment and are shown in Table 12. The Reynolds number suggest that the flows are all in the laminar regime. The results also show that the required entrance length is much larger for flows at the same pressure with NG than for flows with H_2.

Table 12: Calculated entrance length and Reynolds number for a needle valve that is opened two full revolutions

Pressure (kPa)	Reynolds Number		Entrance Length (mm)	
	H_2	NG	H_2	NG
6.89	6.07	21.2	0.282	0.988
13.8	9.56	29.5	0.445	1.37
20.7	13.0	49.8	0.603	2.32
27.6	17.1	62.4	0.796	2.91
34.5	19.7	77.2	0.920	3.59
41.4	23.6	90.1	1.10	4.20
48.3	28.5	105	1.33	4.89
55.2	32.7	121	1.52	5.64
62.1	37.4	136	1.74	6.36
69.0	41.1	146	1.91	6.81

5.6 Packed Capillary Tube Test Results

Finally, the results for the packed capillary tube tests are shown in Figure 27 and Table 13. These results clearly demonstrate that the flowrate of H_2 and NG through this packed capillary tube column is nearly identical for the range of pressure tested. Further, the leakage ratio ranges from 0.99 to 1.07 which is significantly below the leakage rate expected using laminar flow theory. These results more closely replicate the findings observed in our experiments using existing NG infrastructure and the historical findings in [36] that demonstrate H_2 and NG can leak at the same rate. This type of flow cannot be modelled accurately using classical fluid dynamics theories for continuous flow. This suggests that the flow path through the threaded fittings most likely involves a very tortuous path that governs the flow mechanism of the gases. The findings from this experiment lead us to propose a possible explanation for the mechanism of gaseous fuel leakage in the following section.

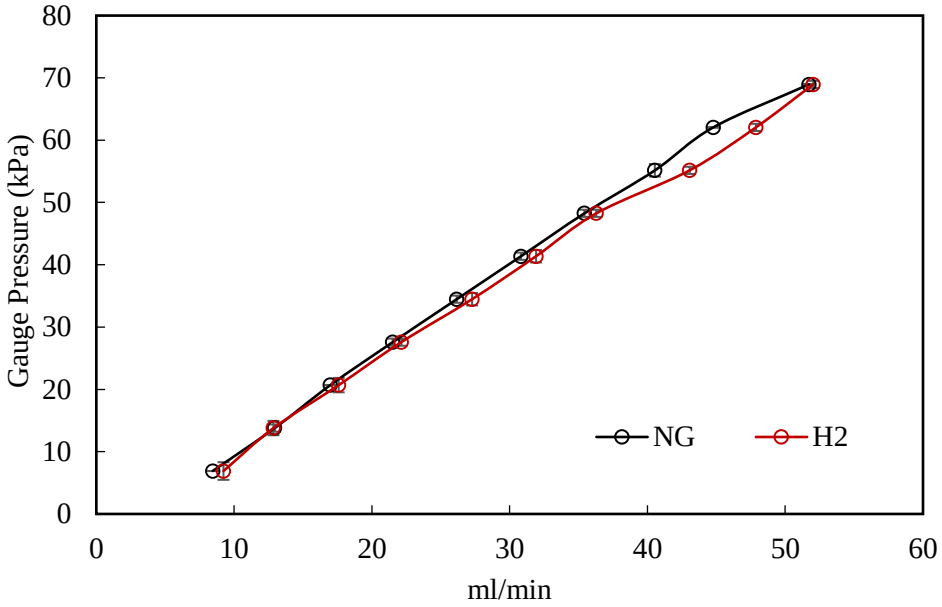

Figure 27: Packed capillary tube test results for NG and H_2

Table 13: Leakage ratio of packed capillary column tests

Pressure	NG	H_2	Leakage Ratio (H_2/NG)
kPa	ml/min	ml/min	
6.9	8.45	8.87	1.05
14	12.95	12.86	0.99
21	16.98	17.59	1.04
28	21.51	22.13	1.03
34	26.16	27.27	1.04
41	30.82	31.91	1.04
48	35.43	36.29	1.02
55	40.54	43.06	1.06
62	44.78	47.87	1.07
69	51.72	52.02	1.01

5.7 Proposed Mechanistic Model for Gaseous Fuel Leakage of H_2 and NG

Based on the results presented in this study and both historical data from the seminal leakage paper and results from independent experiments, it can be concluded that

equations that govern traditional macroscopic, continuous flow regimes do not accurately describe typical leaks in low-pressure NG infrastructure. For the continuum assumption to be valid the molecules must be in thermodynamic equilibrium. Similar to what Ge and Sutton observed in [59] and Swain and Swain observed in [36], it was also observed that gaseous fuel leaks in low-pressure NG infrastructure are mostly due to defects in the threaded connections of commercial (NPT) steel pipe fittings.

NPT fittings have tapered internal and external threads that are designed to form a mated screw connection. When the fitting is torqued the "flanks of the threads compress against each other" [74] and a seal is formed by the metal-to-metal contact of the screw surfaces. Since the threads first make contact at the sides, or flanks, of the threads, a cavity is formed at the roots of the threads. The voids become part of a potential spiral leak path that is typically filled using a thread lubricant or sealant [74]. The ability of fittings to properly seal depends on the integrity of the external and internal threads, the applied torque (over torqueing may damage the threads), the impact and vibration of the piping system, the alignment of the internal and external threads, manufacturing errors, and the ability of the thread sealant to fill the voids in the thread roots. Errors in manufacturing and installation, and degradation may result in enhanced surface roughness on the threads which may offset the alignment and create a potential highly tortuous leak path.

It is proposed that the mechanism of a gas leakage through a fitting in a low-pressure piping system can be characterized by a two-step mechanism that governs leakage rate as follows:

1) In order for a molecule to enter the leakage path, it must first contact the leak crack entrance, enter and remain in the volume of fluid that is present at the crack

entrance. A conceptual rendering of a pipe cross-section leak crack is presented in Figure 28 with the leak crack entrance highlighted and enlarged in the gray circle. The leak crack between the fittings exists within the boundary layer of the piping enclosure. Note, that rarefaction or kinetic effects first appear as slip motion near the wall invalidating the no-slip boundary condition (the assumption that the molecules are moving at the same speed as the boundary) [71]. The molecules that escape through the crack must dissociate themselves from the bulk gaseous molecules and collide with the exact location of the "leak entrance." The molecules that continue to travel through the leakage path between the screw connections, must depart from the equilibrium state. This may occur when the attractive forces between the molecules and wall boundary are sufficiently strong. However, the molecules will be moving in and out of the entrance of the leak path due to attractive and repulsive forces. Therefore, it can be hypothesized that the net movement of the H_2 molecules toward and away from the leak crevice must occur at the same rate as the CH_4 molecules. Although H_2 molecules are more mobile, H_2 molecules move both toward and away from the leak entrance at a faster rate than the CH_4 molecules. Thus, in the absence of a concentration gradient or pressure gradient in this regime, the net rate of molecules entering the crack entrance is the same for all gases.

2) Once the molecules are in the leak path, the second step of the leakage mechanism is governed by a pressure gradient, rather than a concentration gradient because the mixture that enters is consistently present along the leak path until the very exit of the leak (see Figure 28). When the molecules continue to move into the crack, this section of the leak can be described as a tortuous, labyrinth type of leak similar to

what Swain and Shriber describe in [51]. Rough surface conditions on the threads will make the leakage path tortuous it will affect the diffuse reflection of all the molecules and as a result the frequency of wall collisions will increase. This intensification of interactions between the molecules and the wall boundary will cause the molecules in the leak path to deviate from equilibrium, invalidating all continuum flow regime assumptions. In addition, due to the variations of surface roughness on the threads, the cross-sectional area of the leakage path will not be constant. This will result in enhanced tortuosity and in significant density fluctuations throughout the entire length of the path. The fluctuations in the cross-sectional area and in the density suggests that the flow may need to be modelled using multiple molecular flow regimes (e.g., the flip flow regime and the transition flow regime). Therefore, it can be hypothesized that due to the significant tortuosity in the leakage path which intensifies the molecular-wall collisions, the continuum flow regime cannot be used to model these leaks, and all of the molecules in the leakage path will move at the same net rate. Even if H_2 is more mobile than other gases it will simply result in more wall collisions per unit time in direct proportion to mobility so that the net flow is the same for all molecules. Since the mean free path is a conceptual parameter that is used to describe the distance travelled by a molecule in the continuum flow regime and since it cannot be defined for flows where the intermolecular forces are not-well defined [71], the classical understanding of mean free path is not well- defined for these tortuous leak flows and it does not apply here.

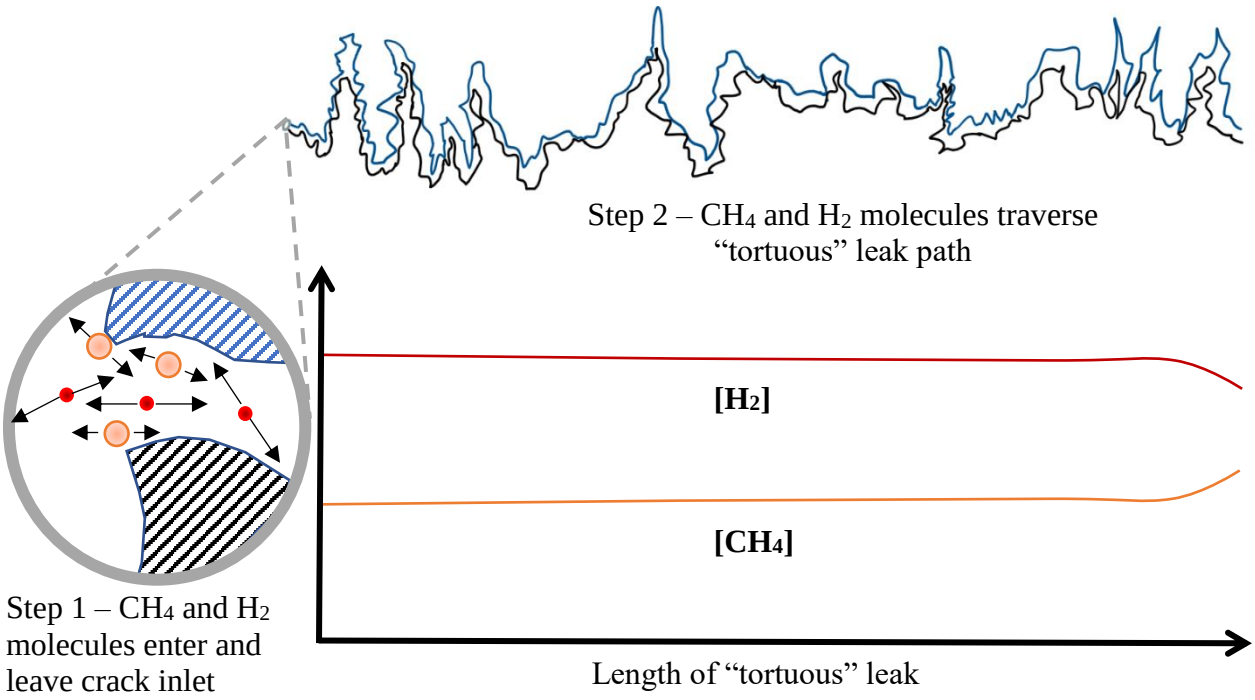

Figure 28: Leakage mechanism steps 1 and 2; the concentration of CH_4 and H_2 is constant until the end of the tortuous leak path when diffusion dominates the flow due to a concentration gradient between the gaseous fuel mixture and ambient air

6 Discussion

In this thesis experimental evidence using existing NG infrastructure and simulated leak systems is provided that suggests H_2, H_2/ NG mixtures and NG all leak at the same rate from fittings in low-pressure NG systems. A review of the literature resulted in the discovery of similar results in [36], one of the few papers that experimentally assesses gaseous fuel leakage from NG infrastructure. Since the majority of practical leaks found in low-pressure NG infrastructure are observed to occur in between pipe fittings and pipe joints in this study and in [36], [59], the fluid flow models associated with this type of fluid flow are best characterized by molecular transport models. It is likely that due to the inherent characteristics of the mated screw connections found in pipe fittings that the gaseous fuel leaks cannot be accurately modelled as fluid flows in the continuum flow regime.

A packed capillary tube was used to produce conditions of tortuous path flow that involves a high rate of wall collisions, which results are shown to replicate the results of the same leakage flow rates for H_2 and NG. Based on these results, it can be hypothesized that gaseous fuel leakage through defects in the mated screw fitting connections that are typical of low-pressure NG infrastructure is governed by a two-step mechanism that involves the molecular dynamics for molecules entering the leak path and flow driven by a pressure gradient and dominated by wall interactions of molecules in the tortuous leak path. As the molecules flow through the tortuous leak path, they will have significantly more interactions with the wall boundary than with other molecules so that the flow deviates from equilibrium and the continuum flow regime cannot be used to accurately model the flow. Additionally, it is likely that the dimensions of the tortuous leakage path will vary

along the length, and thus modelling the leakage path must involve simulation of a variety of flow regimes that typically deviate from the continuum models, and instead are best modelled using molecular dynamics and transport models.

Lastly, an additional finding from this study, is that odorants that are intended to provide an early warning system for detection of leakage were ineffective at identifying sections of NG infrastructure as they leaked very slowly. Small gas leaks from NG infrastructure may produce odorant concentrations that are too low to be detected by olfactory sense. While these leaks do not produce a combustible mixture safety hazard, these small, undetectable, and unintended gas leaks from fittings in low-pressure NG infrastructure may be currently occurring throughout the residential, commercial and industrial sectors of the NG system. The aggregate amount of these leaks could sum up to something significant and may explain some of the discrepancies between bottom-up methane inventories and measured methane concentrations in urban environments [75]. Finally, understanding how H_2 impacts existing NG infrastructure is essential if the NG grid is going to evolve into a renewable gas system that is completely renewable and with zero emissions. It is necessary to understand how H_2 will impact all components of the NG grid, especially those that are in close proximity to consumers.

7 Summary and Conclusions

7.1 Summary

To summarize this thesis:

1. Results presented in this study and historical data from a previous study suggest that equations that govern traditional macroscopic, continuous flow regimes do not accurately describe typical leaks in low-pressure NG infrastructure.
2. Experimental results from previous published studies and from this thesis suggest that H_2 and CH_4 will leak at the same rate from practical leaks from current low-pressure NG infrastructure.
3. H_2 does not preferentially leak from typical faulty low-pressure NG piping infrastructure when mixed with NG.
4. Entrance effects do not explain the similar leakage rates that Swain and Swain observed because our measured entrance effect experiments showed higher H_2 leakage ratios than those expected by laminar flow theories.
5. One mitigation strategy was evaluated and shown to prevent leaks of both H_2 and CH_4.
6. A two-step mechanism theory for gaseous fuel leakage is proposed.

7.2 Conclusions

The results of this study suggest the following conclusions:

1. H_2 and CH_4 may leak at the same rate from low-pressure NG piping infrastructure when the leaks occur through the threaded connections between joints.
2. A two-step mechanism is proposed to understand gaseous leakage under these circumstances that involves (1) molecular dynamics that govern molecule entrance

into the crack, followed by (2) a tortuous flow path with significant wall interactions that dominate the pressure driven flow within the leak path (in which wall collisions per unit time are in direct proportion to mobility so that the net leakage rate is the same for all molecules).

3. Odorants in NG that are intended as an early detection of gaseous fuel leakage are not sufficient to detect small leaks in low pressure infrastructure.
4. The NG system on the customer-side of the meter is a potential source of anthropogenic fossil CH_4 emissions that should be more thoroughly analyzed and perhaps accounted for in official CH_4 inventories.

7.3 Recommendations

Future work should include the following:

1. An experimental analysis which investigates gaseous fuel leakage phenomena through plastic and other types of common pipe materials.
2. A molecular dynamics model to study the effect of tortuosity and significant wall interactions on the flow path of gases and investigate the two-step leakage mechanism proposed in this thesis.
3. An estimate to quantify CH_4 emissions from undetected leakage in infrastructure on the customer-side-of the meter.

8 References

[1] W. Steffen, J. Grinevald, P. Crutzen, and J. Mcneill, "The Anthropocene: conceptual and historical perspectives," *Philos. Trans. R. Soc. London A Math. Phys. Eng. Sci.*, vol. 369, no. 1938, pp. 842–867, 2011.

[2] T. W. Donovan, "9 Worst Coal Mine Catastrophes (PHOTOS) | HuffPost," *Huffington Post*, 2010. [Online]. Available: https://www.huffingtonpost.com/2010/04/15/9-worst-coal-mine-catastr_n_537890.html. [Accessed: 30-Jun-2018].

[3] J. C. Castaneda, "Natural Disasters in the Making: Fossil Fuels, Humanity, and the Environment," *OAH Mag. Hist.*, vol. 25, no. 4, pp. 21–25, Oct. 2011.

[4] P. J. Crutzen, "The 'Anthropocene,'" in *Earth System Science in the Anthropocene*, Berlin, Heidelberg: Springer, 2006, pp. 13–18.

[5] J. P. Crutzen., "Geology of Mankind," *Nature*, vol. 415, no. 6867, p. 23, 2002.

[6] S. L. Lewis and M. A. Maslin, "Defining the Anthropocene," *Nature*, vol. 519, no. 7542, pp. 171–180, 2015.

[7] U.S. Energy Information Administration, *International Energy Outlook 2016*, vol. 0484(2016), no. May 2016. 2016.

[8] "Assembly Bill 32 Overview," *California Air Resources Board*, 2014. [Online]. Available: https://www.arb.ca.gov/cc/ab32/ab32.htm. [Accessed: 22-Aug-2017].

[9] "California Senate Leader Introduces 100 Percent Clean Energy Measure," 2017. [Online]. Available: http://sd24.senate.ca.gov/news/2017-05-02-california-senate-leader-introduces-100-percent-clean-energy-measure. [Accessed: 22-Aug-2017].

[10] "AB 617 Background," *Air Quality Management District*, 2017. [Online]. Available: http://www.airquality.org/air-quality-health/community-air-protection/ab-617-background. [Accessed: 16-Jul-2019].

[11] S. Hardman *et al.*, "Driving the Market for Plug-in Vehicles : Understanding ZEV Mandates," Davis, 2018.

[12] M. J. Coren, "California's 2018 legislative blitzkrieg delivered its most ambitious climate policies ever," *Quartz*, 2018. [Online]. Available: https://qz.com/1409065/californias-2018-legislative-blitzkrieg-delivered-its-most-ambitious-climate-policies-ever/. [Accessed: 17-Jul-2019].

[13] G. Gahleitner, "Hydrogen from renewable electricity: An international review of power-to-gas pilot plants for stationary applications," *Int. J. Hydrogen Energy*, vol. 38, no. 5, pp. 2039–2061, 2013.

[14] J. Auer, "E.ON inaugurates first 2 MW Power-to-Gas unit in Falkenhagen," *Fuel Cells Bull.*, vol. 2013, no. 9, p. 9, 2013.

[15] Q. Schiermeier, "Germany's Energy Gamble," *Nature*, vol. 496, pp. 156–158, 2013.

[16] S. J. Davis *et al.*, "Net-zero emissions energy systems," *Science (80-.).*, vol. 360, no. 6396, 2018.

[17] D. Cusick, "Wind and Solar Growth Outpace Gas - Scientific American," 2017. [Online]. Available: https://www.scientificamerican.com/article/wind-and-solar-growth-outpace-gas/. [Accessed: 04-Aug-2017].

[18] P. Denholm, M. O'Connell, G. Brinkman, and J. Jorgenson, "Overgeneration from Solar

Energy in California: A Field Guide to the Duck Chart (NREL/TP-6A20-65023)," *Tech. Rep.*, no. November, p. 46, 2015.

[19] P. Denholm, R. Margolis, and J. Milford, "Production Cost Modeling for High Levels of Photovoltaics Penetration," 2008.

[20] B. Speer *et al.*, "The Role of Smart Grids in Integrating Renewable Energy," 2015.

[21] E. (E3) Cutter, "Valuing Energy Storage as a Flexible Resource: Final Phase 1 Report for Consideration in CPUC A. 14-02-006," pp. 1–30, 2014.

[22] F. Díaz-González, A. Sumper, O. Gomis-Bellmunt, and R. Villafáfila-Robles, "A review of energy storage technologies for wind power applications," *Renew. Sustain. Energy Rev.*, vol. 16, no. 4, pp. 2154–2171, 2012.

[23] J. D. Maclay, J. Brouwer, and G. Scott Samuelsen, "Dynamic analyses of regenerative fuel cell power for potential use in renewable residential applications," *Int. J. Hydrogen Energy*, vol. 31, no. 8, pp. 994–1009, 2006.

[24] M. Beaudin, H. Zareipour, A. Schellenberglabe, and W. Rosehart, "Energy storage for mitigating the variability of renewable electricity sources: An updated review 10.1016/j.esd.2010.09.007 : Energy for Sustainable Development | ScienceDirect.com," *Energy Sustain. Dev.*, vol. 14, no. 4, pp. 302–314, 2010.

[25] W. F. Pickard, A. Q. Shen, and N. J. Hansing, "Parking the power: Strategies and physical limitations for bulk energy storage in supply–demand matching on a grid whose input power is provided by intermittent sources," *Renew. Sustain. Energy Rev.*, vol. 13, no. 8, pp. 1934–1945, Oct. 2009.

[26] E. Wagner, “Economics of Power to Gas.”

[27] M. Götz *et al.*, “Renewable Power-to-Gas: A technological and economic review,” *Renewable Energy*, vol. 85. pp. 1371–1390, 2016.

[28] S. Schiebahn, T. Grube, M. Robinius, V. Tietze, B. Kumar, and D. Stolten, “Power to gas: Technological overview, systems analysis and economic assessment for a case study in Germany,” *Int. J. Hydrogen Energy*, vol. 40, no. 12, pp. 4285–4294, 2015.

[29] “E.ON inaugurates first 2 MW Power-to-Gas unit in Falkenhagen,” *Fuel Cells Bull.*, vol. 2013, no. 9, p. 9, Sep. 2013.

[30] M. Bailera, P. Lisbona, L. M. Romeo, and S. Espatolero, “Power to Gas projects review: Lab, pilot and demo plants for storing renewable energy and CO2,” *Renewable and Sustainable Energy Reviews*, vol. 69. pp. 292–312, Mar-2017.

[31] “Hydrogenics Awarded 2.4 MW Power-to-Gas Plant in Germany | Hydrogenics,” 2017. [Online]. Available: http://www.hydrogenics.com/2017/03/22/hydrogenics-awarded-2-4-mw-power-to-gas-plant-in-germany/. [Accessed: 10-Aug-2017].

[32] J. de (enea consulting) Bucy, “The Potential of Power-To-Gas,” 2016.

[33] “Hydrogenics selected for 2 MW Ontario energy storage facility,” *Fuel Cells Bull.*, vol. 2014, no. 8, p. 9, Aug. 2014.

[34] “UC Irvine injects P2G green hydrogen into campus power supply,” *Fuel Cells Bulletin*, vol. 2017, no. 1. Elsevier Advanced Technology, p. 10, 01-Jan-2017.

[35] M. Dadfarnia, P. Sofronis, J. Brouwer, and S. Sosa, “Assessment of resistance to fatigue

crack growth of natural gas line pipe steels carrying gas mixed with hydrogen," *Int. J. Hydrogen Energy*, vol. 44, no. 21, pp. 10808–10822, Apr. 2019.

[36] M. R. Swain and M. N. Swain, "A comparison of H2, CH4 and C3H8 fuel leakage in residential settings," *Int. J. Hydrogen Energy*, vol. 17, no. 10, pp. 807–815, 1992.

[37] M. W. Melaina, O. Antonia, and M. Penev, "Blending Hydrogen into Natural Gas Pipeline Networks : A Review of Key Issues Blending Hydrogen into Natural Gas Pipeline Networks : A Review of Key Issues," 2013.

[38] R. W. Schefer, W. G. Houf, C. San Marchi, W. P. Chernicoff, and L. Englom, "Characterization of leaks from compressed hydrogen dispensing systems and related components," *Int. J. Hydrogen Energy*, vol. 31, no. 9, pp. 1247–1260, 2006.

[39] A. G. Venetsanos, D. Baraldi, P. Adams, P. S. Heggem, and H. Wilkening, "CFD modelling of hydrogen release, dispersion and combustion for automotive scenarios," *J. Loss Prev. Process Ind.*, vol. 21, no. 2, pp. 162–184, 2008.

[40] A. Saeedmanesh, M. A. Mac Kinnon, and J. Brouwer, "Hydrogen is essential for sustainability," *Curr. Opin. Electrochem.*, vol. 12, pp. 166–181, 2018.

[41] N. Mejia Hormaza and J. Brouwer, "Gaseous Fuel Leakage from Natural Gas Infrastructure," in *International Mechanical Engineering Congress and Exposition*, 2018, pp. 1–6.

[42] G. Muller-Syring *et al.*, "Power to gas: Untersuchungen im Rahmen der DVGW-Innovationsoffensive zur Energiespeicherungitle," 2011.

[43] "U.S. Energy Facts - Energy Explained," *U.S Energy Information Administration*, 2018.

[Online]. Available: https://www.eia.gov/energyexplained/?page=us_energy_home. [Accessed: 29-Jan-2019].

[44] "Natural Gas Pipelines - Energy Explained, Your Guide To Understanding Energy - Energy Information Administration." [Online]. Available: https://www.eia.gov/energyexplained/index.php?page=natural_gas_pipelines. [Accessed: 08-Aug-2018].

[45] "Natural Gas Basics," *US Energy Information Administration*. [Online]. Available: https://www.eia.gov/kids/energy.php?page=natural_gas_home-basics. [Accessed: 29-Jan-2019].

[46] H. de Vries, A. V. Mokhov, and H. B. Levinsky, "The impact of natural gas/hydrogen mixtures on the performance of end-use equipment: Interchangeability analysis for domestic appliances," *Appl. Energy*, vol. 208, no. August, pp. 1007–1019, 2017.

[47] Y. Zhao, V. McDonell, and S. Samuelsen, "Influence of hydrogen addition to pipeline natural gas on the combustion performance of a cooktop burner," *Int. J. Hydrogen Energy*, vol. 44, no. 23, pp. 12239–12253, 2019.

[48] D. Vries, N. V. N. Gasunie, P. O. Box, and M. A. Groningen, "Safe Operation of Natural Gas Appliances Fueled With Hydrogen/Natural Gas Mixtures (Progress Obtained in the Naturalhy-Project)," *Int. Conf. Saf. Hydrog.*, pp. 1–12, 2007.

[49] J. Ivy, "Summary of Electrolytic Hydrogen Production: Milestone Completion Report," 2003.

[50] "Use of Natural Gas - Energy Explained, Your Guide To Understanding Energy -

Energy Information Administration." [Online]. Available: https://www.eia.gov/energyexplained/index.php?page=natural_gas_use. [Accessed: 29-Nov-2018].

[51] M. R. Swain and J. Shriber, "Comparison of Hydrogen, Natural Gas, Liquified Petroleum Gas, and Gasoline Leakage in a Residential Garage," *Energy & Fuels*, vol. 12, pp. 83–89, 1998.

[52] J. Newton, "Power-to-Gas & Methanation - Pathways to a Hydrogen Economy," *14TH Annu. APGTF Work. London*, no. March, pp. 12–13, 2014.

[53] K. Altfeld and D. Pinchbeck, "Admissible hydrogen concentrations in natural gas systems," *Gas Energy*, vol. March/2013, pp. 1–16, 2013.

[54] S. Choudhury, Y. Zhao, and V. G. Mcdonell, "Combustion performance of storage water heaters operated on mixtures of natural and renewable gas," *11th U. S. National Combustion Meeting Organized by the Western States Section of the Combustion Institute*, no. April. pp. 1–8, 2019.

[55] M. Gad-el-Hak, "The Fluid Mechanics of Microdevices — The Freeman Scholar Lecture," *J. Fluids Eng.*, vol. 121, no. 1, pp. 5–33, 1999.

[56] S. G. Kandlikar, S. Garimella, D. Li, S. Colin, and M. King, "Heat Transfer and Fluid Flow in Minichannels and Microchannels," *Heat Transfer and Fluid Flow in Minichannels and Microchannels*. pp. 1–555, 2013.

[57] S. V. Patankar, C. H. Liu, and E. M. Sparrow, "Fully Developed Flow and Heat Transfer in Ducts Having Streamwise-Periodic Variations of Cross-Sectional Area," *J. Heat*

Transfer, vol. 99, no. 2, p. 1, 1977.

[58] P. E. Liley *et al.*, *Perry's Chemical Engineers' Handbook*, 7th ed. McGraw-Hill.

[59] X. Ge and W. H. Sutton, "Analysis and Test of Compressed Hydrogen Interface Leakage by Commercial Stainless Steel (NPT) Fittings," *SAE Tech. Pap. 2006-01-0130*, 2006.

[60] Y. Qi, X. Meng, D. Mu, Y. Sun, and H. Zhang, "Study on mechanism and factors affecting the gas leakage through clearance seal at nano-level by molecular dynamics method," *Energy*, vol. 102, pp. 252–259, 2016.

[61] J. Pangborn, M. Scott, and J. Sharer, "Technical Prospects for Commercial and Residential Distribution and Utilization of Hydrogen," *Int. J. Hydrogen Energy*, vol. 2, pp. 431–445, 1977.

[62] "Sizing and Capacities of Gas Piping." Internation Residential Code 2006, New Jersey Edition, 2006.

[63] "NaturalGas.org," 2013. [Online]. Available: http://naturalgas.org/naturalgas/distribution/. [Accessed: 13-Apr-2017].

[64] Z. Y. Guo and X. B. Wu, "Further Study on Compressibility Effects on the Gas Flow and Heat Transfer in a Microtube," *Microscale Thermophys. Eng.*, vol. 2, pp. 111–120, 1998.

[65] T. L. Bergman, A. S. Lavine, F. P. Incropera, and D. P. Dewitt, *Fundamentals of Heat and Mass Transfer*, 7th ed., no. c. John Wiley & Sons Inc., 2011.

[66] J. Welty, C. E. Wicks, G. L. Rorrer, and R. E. Wilson, *Fundamentals of Momentum, Heat, and Mass Transfer*. 2006.

[67] M. F. White, *Fluid Mechanics*, 7th ed. New York, NY, USA: McGraw-Hill, 2011.

[68] S. G. Kandlikar, S. Garimella, D. Li, S. Colin, and M. King, "Heat Transfer and Fluid Flow in Minichannels and Microchannels," *Heat Transfer and Fluid Flow in Minichannels and Microchannels*. pp. 1–555, 2013.

[69] S. Colin, "Rarefaction and compressibility effects on steady and transient gas flows in microchannels," *Microfluid. Nanofluidics*, vol. 1, no. 3, pp. 268–279, 2005.

[70] A. Akbarinia, "Simulation and Modeling of Microfluidic Systems," Universität Bremen, 2013.

[71] S. H. Kim, H. Pitsch, and I. D. Boyd, "Slip velocity and Knudsen layer in the lattice Boltzmann method for microscale flows," *Phys. Rev. E - Stat. Nonlinear, Soft Matter Phys.*, vol. 77, no. 2, pp. 1–12, 2008.

[72] D. A. Lockerby, J. M. Reese, and M. A. Gallis, "The usefulness of higher-order constitutive relations for describing the Knudsen layer," *Phys. Fluids*, vol. 17, no. 100609, p. 3061, 2005.

[73] Z. L. Guo, B. C. Shi, and C. G. Zheng, "An extended Navier-Stokes formulation for gas flows in the Knudsen layer near a wall," *EPL (Europhysics Lett.*, vol. 80, no. 2, 2007.

[74] G. Wright, O. C. Duffy, and S. A. Heard, *Fundamentals of Mobile Heavy Equipment*. Jones & Bartlett Learning, 2017.

[75] S. M. Miller *et al.*, "Anthropogenic emissions of methane in the United States.," *Proc. Natl. Acad. Sci. U. S. A.*, vol. 110, no. 50, pp. 20018–22, 2013.